DEUTSCHES ELEKTRONEN – SYNCHROTRON

DESY 93–005
January 1993

Measurement of Inclusive Semileptonic B Decays with the ARGUS Detector

A. Nau

Deutsches Elektronen-Synchrotron DESY, Hamburg

ISSN 0418-9833

NOTKESTRASSE 85 · D-2000 HAMBURG 52

To be sure that your preprints are promptly included in the
HIGH ENERGY PHYSICS INDEX,
send them to (if possible by air mail):

DESY **Bibliothek** **Notkestraße 85** **W-2000 Hamburg 52** **Germany**	**DESY-IfH** **Bibliothek** **Platanenallee 6** **O-1615 Zeuthen** **Germany**

DESY 93-005
January 1993

ISSN 0418-9833

Measurement of Inclusive Semileptonic B Decays with the ARGUS Detector

Dissertation
zur Erlangung des Doktorgrades
des Fachbereiches Physik
der Universität Hamburg

vorgelegt von
ANDREAS NAU
aus Hamburg

Hamburg
1992

Gutachter der Dissertation:	Prof. Dr. W. Schmidt-Parzefall Prof. Dr. V. Sörgel
Gutachter der Disputation:	Prof. Dr. W. Schmidt-Parzefall Prof. Dr. E. Lohrmann
Datum der Disputation:	21.12.1992
Sprecher des Fachbereichs Physik und Vorsitzender des Promotionsausschusses:	Prof. Dr. G. Mack

Abstract

Using data collected with the ARGUS detector at the e^+e^- storage ring DORIS II at DESY, the inclusive semileptonic branching ratio of B mesons, the charm content of the final hadronic state and $|V_{cb}|$ have been measured.

Model-dependent inclusive semileptonic branching ratios of B mesons are obtained by fitting theoretical models to measured and corrected lepton spectra. Using the free-quark model gives $BR(B \to Xl\nu) = (9.4 \pm 0.1 \pm 0.6)\,\%$ and $|V_{cb}| = 0.041 \pm 0.001 \pm 0.002$, the model of Altarelli et al. $BR(B \to Xl\nu) = (9.7 \pm 0.2 \pm 0.6)\,\%$ and $|V_{cb}| = 0.041 \pm 0.001 \pm 0.002$, the one of Grinstein et al. $BR(B \to Xl\nu) = (9.5 \pm 0.1 \pm 0.6)\,\%$ and $|V_{cb}| = 0.042 \pm 0.001 \pm 0.006$, and a modified version of the Grinstein et al. model with free D^{**} content $BR(B \to Xl\nu) = (9.7 \pm 0.5 \pm 0.6)\,\%$ and $|V_{cb}| = 0.043 \pm 0.006 \pm 0.002$ where l is either an electron or a muon. The first quoted error on the semileptonic branching ratio is statistical and the second systematic, whereas the first error on $|V_{cb}|$ is experimental and the second theoretical.

A 'model-independent' inclusive semileptonic branching ratio for B mesons and $|V_{cb}|$ are obtained by tagging electrons with D^0 and D^{*+} mesons. The results are: $BR(B \to Xe\nu) = (11.2 \pm 2.8 \pm 1.1)\,\%$ and $|V_{cb}| = 0.045 \pm 0.006 \pm 0.002$.

Counting the charm fraction in the final hadronic state in semileptonic B decays with lepton momenta greater than $1.2\,GeV/c$ yields $(97 \pm 11 \pm 8)\,\%$.

Kurzfassung

Unter Verwendung von Daten, die mit dem ARGUS-Detektor am e^+e^--Speicherring DORIS II bei DESY aufgezeichnet worden sind, ist das inklusive semileptonische Verzweigungsverhältnis von B Mesonen, der Charmanteil im hadronischen Endzustand und $|V_{cb}|$ gemessen worden.

Modellabhängige inklusive semileptonische Verzweigungsverhältnisse von B Mesonen werden durch Anpassungsrechnungen von theoretischen Modellen an gemessene und korrigierte Leptonspektren erhalten. Das freie Quarkmodell ergibt $BR(B \to Xl\nu) = (9.4 \pm 0.1 \pm 0.6)\,\%$ und $|V_{cb}| = 0.041 \pm 0.001 \pm 0.002$, das Modell von Altarelli et al. $BR(B \to Xl\nu) = (9.7 \pm 0.2 \pm 0.6)\,\%$ und $|V_{cb}| = 0.041 \pm 0.001 \pm 0.002$, das von Grinstein et al. $BR(B \to Xl\nu) = (9.5 \pm 0.1 \pm 0.6)\,\%$ und $|V_{cb}| = 0.042 \pm 0.001 \pm 0.006$ und eine modifizierte Version des Grinstein et al. Modells mit freien D^{**} Anteil $BR(B \to Xl\nu) = (9.7 \pm 0.5 \pm 0.6)\,\%$ und $|V_{cb}| = 0.043 \pm 0.002 \pm 0.006$, wobei l entweder ein Elektron oder Myon ist. Der erste angegebene Fehler des semileptonischen Verzweigungsverhältnisses ist der statistische, der zweite der systematische, wohingegen bei $|V_{cb}|$ der erste Fehler experimentelle Unsicherheiten sind und der zweite theoretische.

Ein 'modellunabhängiges' inklusives semileptonisches Verzweigungsverhältnis von B Mesonen und $|V_{cb}|$ werden durch Taggen von Elektronen mit D^0 und D^{*+} Mesonen erhalten. Das Resultate lauten: $BR(B \to Xe\nu) = (11.2 \pm 2.8 \pm 1.1)\,\%$ und $|V_{cb}| = 0.045 \pm 0.002 \pm 0.006$.

Das Messen des Charmanteils im hadronischen Endzustand von semileptonischen B Zerfällen mit Leptonimpulsen größer als $1.2\,GeV/c$ ergibt $(97 \pm 11 \pm 8)\,\%$.

Contents

List of Figures

List of Tables

Introduction

"It peaks at all masses."
T. Hamacher, 1992

Semileptonic decays of B mesons are of special interest in the physics of B mesons. They are sensitive to two fundamental parameters of the standard model, the Cabibbo-Kobayashi-Maskawa matrix elements V_{cb} and V_{ub}. The absolute values of V_{cb} and V_{ub} determine the rate of semileptonic B decays.

Different Feynman graphs of weak B meson decays are shown Figure .1. The spectator decay width (a), which is proportional to m_b^5, should dominate over the exchange (b) and annihilation (c) width, which are proportional to $m_b^5(m_q/m_b)^2$, where m_b and m_q are the masses of the b and the decay product quark q [28]. Penguin graphs (d) should have no significant contribution to B decays [2].

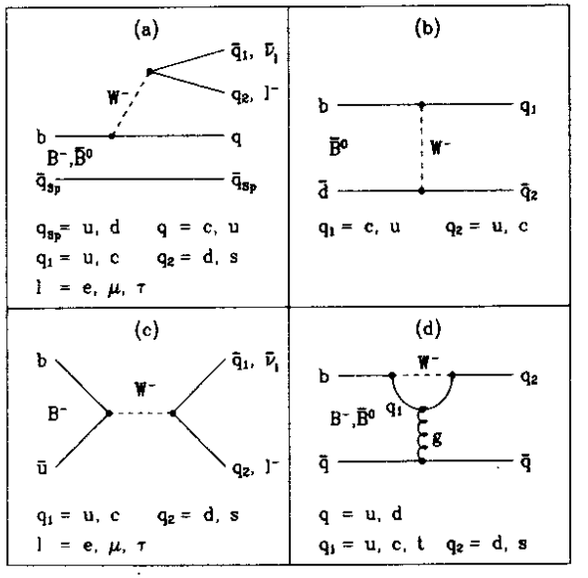

Figure .1: *Different Feynman graphs of B meson decays: spectator (a), W exchange (b), annihilation (c), and penguin graph (d).*

The most simple calculation of the inclusive semileptonic branching ratio of B mesons can be done in the spectator picture. Considering all energetically allowed weak decay modes with their phase space factors and assuming $|V_{ub}|$ to be small leads to:

$$BR(B \to Xe\nu) = \frac{(e\nu)}{(e\nu) + (\mu\nu) + 0.3(\tau\nu) + 3[(ud + 0.3(cs)]} = 16\,\% \,. \qquad (.1)$$

More detailed models include gluon radiations. These additional effects lower the semileptonic branching ratio to [33]:

$$BR(B \to Xe\nu) = (12 - 16)\,\% \,. \qquad (.2)$$

In contrast to the simple spectator model recent experimental data show a significantly smaller branching ratio of about $(10.0 \pm 0.6)\%$. Shown in Figure .2 are measurements from different experiments running on the $\Upsilon(4S)$ resonance [13,14,15, 16,17,18,21,37,39]. Although the errors on the first measurements are quite high the pattern is obvious. At the beginning the measurements were close to the predicted values of the simple spectator model but went down with time.

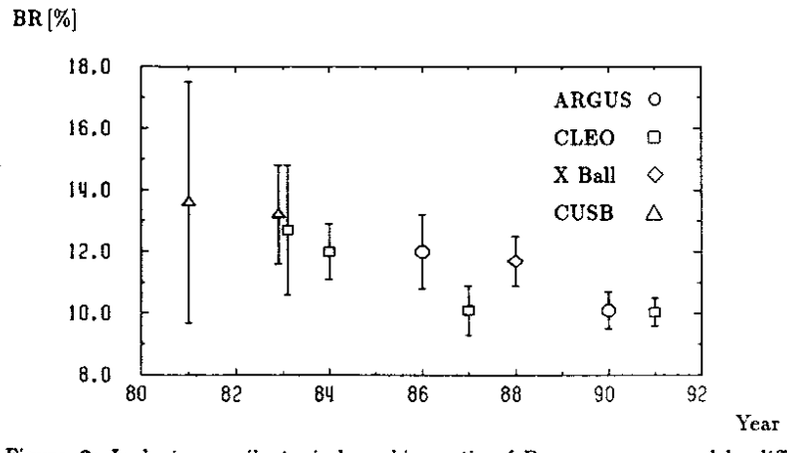

Figure .2: *Inclusive semileptonic branching ratio of B mesons measured by different collaborations running on the* $\Upsilon(4S)$ *resonance* [13,14,15,16,17,18,21,37,39].

The question arises: Why are there differences between experiment and theory ? The answer can be given in two ways, one in a theoretical and one in an experimental direction.

In a recent theoretical review [2] the spectator model was shown to be compatible with an inclusive semileptonic branching ratio of B mesons of $(11.5 - 12.0)\,\%$. A further reduction in the value of the semileptonic branching ratio could be reached by taking into account non spectator effects of B decays. The most plausible mechanism is W exchange with gluon emission. Another possibility is interference effects in hadronic B decays. Penguin diagram terms are small and their contribution to the total hadronic width are further suppressed by strong cancellations.

In the experimental field the following has to be pointed out. The experiments running on the $\Upsilon(4S)$ resonance assume that the $\Upsilon(4S)$ resonance decays 100 % of the

time into $B\bar{B}$ pairs. Any non $B\bar{B}$ contribution to the $\Upsilon(4S)$ decays would increase the semileptonic branching ratio of B mesons as well as other branching ratios. But the search for such non $B\bar{B}$ decays has not been successful up to now [31].

The aim of this work is to measure a more precise inclusive semileptonic branching ratio of B mesons and a more precise absolute value of the Cabibbo-Kobayashi-Maskawa matrix element V_{cb}, with special focus on lowering the model dependence. The thesis is divided into five parts.

In the first Chapter, the theoretical models which are used to fit the measured lepton spectra in Chapter 3 are described: the free-quark model, the model of Altarelli et al. (ACCMM model [1]), and the model of Grinstein et al. (GISW model [20]). Also shown is how the absolute value of the Cabibbo-Kobayashi-Maskawa matrix element V_{cb} is calculated from the inclusive semileptonic branching ratio.

In Chapter 2, the source of data for the ARGUS experiment, the Υ resonances, is described briefly. Subsequently, the ARGUS detector is described and the method of particle identification, especially lepton identification, outlined.

In Chapter 3, the inclusive semileptonic branching ratio of B mesons is determined by fitting theoretical models to the measured and corrected lepton spectra of B mesons. From these inclusive semileptonic branching ratios $|V_{cb}|$ is determined within each model.

In Chapter 4, the semileptonic branching ratio is evaluated without using any theoretical model to describe semileptonic $b \to c$ quark transitions. D^0 and D^{*+} mesons are used to tag leptons coming from $b \to c$ decays. A 'model independent' inclusive semileptonic branching ratio of B mesons can be measured.

In Chapter 5, the charm fraction of semileptonic B meson decays is determined. This is done counting the D^0 and D^+ mesons in the final state.

Chapter 1

Theory

The theoretical models used to describe semileptonic decays of heavy mesons can be divided into spectator and form factor models. Spectator models describe semileptonic decays at the quark level whereas form factor models work at the hadron level.

1.1 Spectator Models

1.1.1 Free-Quark Model

In the free-quark model of B meson decay, the b quark decays via W emission into either a c or a u quark. The other quark in the B meson, the spectator quark, is considered to have no effect on the b quark decay; the b quark is free. In semileptonic decays, the W produces a lepton neutrino pair (compare Figure .1a).

The semileptonic width of the b quark is proportional to the fifth power of the b quark mass:

$$\Gamma_{b\to ql\nu} = \frac{G_F^2 m_b^5}{192\pi^3}\{f_{cb}g_{cb}|V_{cb}|^2 + f_{ub}g_{ub}|V_{ub}|^2\} \tag{1.1}$$

where G_F is the Fermi constant, and m_b the b quark mass. V_{qb}, f_{qb} and g_{qb} denote, respectively, the CKM matrix elements, phase space factors, and corrections due to gluon radiation. The phase space factors f_{qb} are given by [10]:

$$f_{qb}(\epsilon) = 1 - 8\epsilon^2 - 24\epsilon^4 \ln\epsilon + 8\epsilon^6 - \epsilon^8 \tag{1.2}$$

where $\epsilon = m_q/m_b$. The gluon bremsstrahlungs corrections g_{qb} are taken from [11]:

$$g_{qb}(\epsilon) = 1 - \frac{2}{3}\frac{\alpha_S}{\pi}\left(\pi^2 - \frac{25}{4}\right)\left(1 - 1.23\epsilon + 0.7\epsilon^2\right) . \tag{1.3}$$

The free-quark model also predicts the momentum spectrum of the final state fermions. The charged lepton spectrum is given by [1]:

$$\frac{d\Gamma}{dx} = \frac{G^2 m_b^5}{96\pi^3}x^2\frac{(x_m - x)^2}{(1-x)^3}[(1-x)(3-2x) + (1-x_m)(3-x)] \tag{1.4}$$

where $x_m = 1-(m_q/m_b)^2$, the maximum kinematically allowed value for $x = 2E_l/m_b$, and E_l is the energy of the lepton.

The semileptonic decay width of the B meson $\Gamma_{B\to Xl\nu}$ is determined from the lifetime τ_B and the inclusive semileptonic branching ratio:

$$\Gamma_{B\to Xl\nu} = BR(B\to Xl\nu)/\tau_B . \tag{1.5}$$

With the known ratio of $|V_{ub}|/|V_{cb}|$ [9] and identifying the semileptonic decay width of the B meson $\Gamma_{B\to Xl\nu}$ with the one of the b quark $\Gamma_{b\to ql\nu}$, the Cabibbo-Kobayashi-Maskawa matrix element $|V_{cb}|$ can be determined from Equation 1.1 and 1.5:

$$|V_{cb}| = \sqrt{\frac{BR(B\to Xl\nu)}{f_{cb}g_{cb} + f_{ub}g_{ub}|V_{ub}|^2/|V_{cb}|^2}\,\frac{192\pi^3}{G_F^2 m_b^5}\,\frac{1}{\tau_B}} . \tag{1.6}$$

At first sight, $|V_{cb}|$ is proportional to $m_b^{-5/2}$. But due to the phase space factors f_{qb}, this dependence is in fact less severe. According to [35], $|V_{cb}|$ is proportional to $(m_b - m_c)^{-5/2}$.

1.1.2 ACCMM Model

The ACCMM model [1] is a modified free-quark model. In order to improve the free-quark model the authors introduce a relative momentum between the b quark and the spectator quark in the B meson and soft gluon radiations.

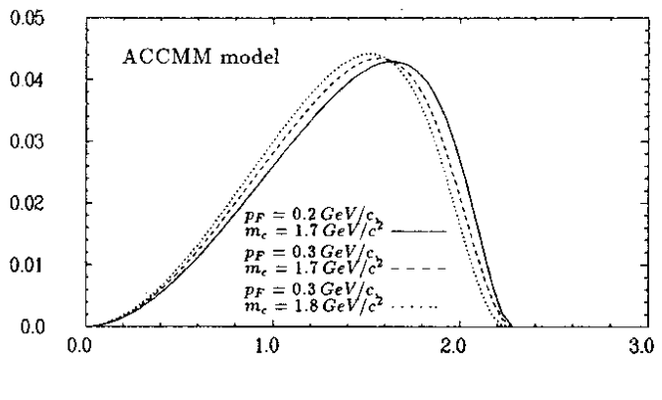

Figure 1.1: *Lepton spectra of inclusive semileptonic B decays of the ACCMM model with different values of p_F and m_c.*

The relative momentum between the b and spectator quark is termed the Fermi momentum. The distribution $\phi(p)$ of the Fermi momentum is assumed to be Gaussian:

$$\phi(p) = \frac{4}{\sqrt{\pi}p_F^3}\exp\left(-\frac{p^2}{p_F^2}\right) . \tag{1.7}$$

The parameter p_F determines the width of the distribution. The spectator quark is treated as a particle of definite mass m_{sp} and momentum p, while the heavy quark is treated as virtual particle of invariant mass $\tilde{m}_b$:

$$\tilde{m}_b^2 = M_B^2 + m_{sp}^2 - 2M_B\sqrt{p^2 + m_{sp}^2} . \tag{1.8}$$

where M_B is the B meson mass. Hence, the ACCMM model has three free parameters: the width of the Fermi momentum p_F, the c quark mass m_c, and the spectator

quark mass m_{sp}. For the calculation of $|V_{cb}|$, a real b quark mass can be obtained from $\bar{m}_b$ with the average momentum $\langle p \rangle = 2p_F/\sqrt{\pi}$:

$$m_b = \langle \bar{m}_b \rangle \simeq m_B - \frac{2p_F}{\sqrt{\pi}} . \tag{1.9}$$

Figure 1.1 shows the lepton momentum spectrum of the ACCMM model with different values of p_F and m_c. The effect of a variation of the p_F parameter is similar to the variation of the final state mass m_c. Larger p_F values soften the spectrum, as do higher m_c values.

The QCD corrections are computed in a leading logarithm approximation. They depend only weakly on the momentum of the lepton and can be treated as constant.

1.2 Form Factor Models

There are many form factor models available to describe semileptonic B decays: [8,20,27,32]. The only model which has calculated $B \to D^{**} l\nu$ decays so far is the GISW model [20]. Form factor models without D^{**} mesons in the final state can not be expected to describe the low momentum part of the lepton spectrum. Therefore, the GISW model is the only form factor model used to fit the lepton spectra in Chapter 3.

1.2.1 GISW Model

Grinstein et al. [20] calculate the decay rates and the momentum spectra for each exclusive $B \to X(J^{PC}) l\nu$ decay. To build up the inclusive spectrum the single exclusive spectra have to be added. The differential decay width in this model is:

$$\begin{aligned} \frac{d^2\Gamma}{dxdy} &= |V_{qb}|^2 \frac{G_F^2 m_B^5}{32\pi^3} \\ &\times \left\{ \frac{\alpha}{m_B^2} y + 2\beta \left[2x \left(1 - \frac{m_X^2}{m_B^2} + y \right) - 4x^2 - y \right] - y\gamma \left[1 - \frac{m_X^2}{m_B^2} - 4x + y \right] \right\} \end{aligned} \tag{1.10}$$

where $x = E_l/m_B$ and $y = t/m_B^2 = (p_B - p_X)^2/m_B^2$. The symbols m_i and p_i denote the masses and 4-momenta of the B and the final state meson X. The form factors α, β and γ are calculated for the transitions to all final states with quantum numbers $1S$, $1P$ and $2S$. The authors use the following quark masses: $m_b = 5.12\,GeV/c^2$, $m_c = 1.82\,GeV/c^2$, and $m_u = m_d = 0.33\,GeV/c^2$, respectively. The decay width for semileptonic $b \to c$ transitions is found to be:

$$\Gamma(B \to X_c l\nu) = 0.41 \cdot 10^{14} |V_{cb}|^2 s^{-1} . \tag{1.11}$$

For $b \to c$ transitions, the amount of D, D^* and D^{**} in the final state comes out to be 27 %, 60 % and 13 %, respectively [20]. The lepton spectrum for each charmed final state can be found in Figure 1.2. The endpoints are determined by the mass differences of the B meson and the final state hadrons.

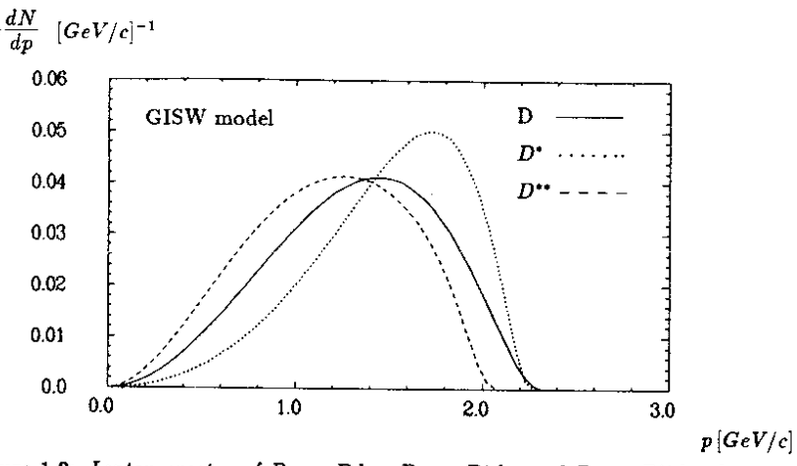

Figure 1.2: *Lepton spectra of $B \to D\,l\nu$, $B \to D^*\,l\nu$ and $B \to D^{**}\,l\nu$ decays of the GISW model.*

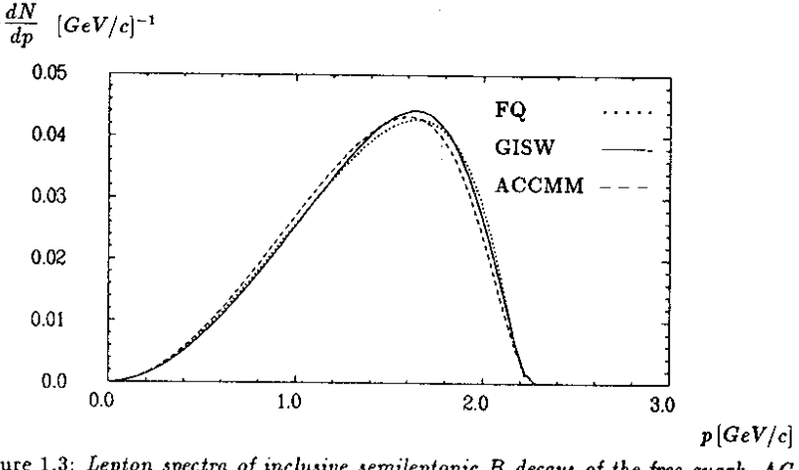

Figure 1.3: *Lepton spectra of inclusive semileptonic B decays of the free-quark, ACCMM and GISW model.*

In Figure 1.3 the inclusive spectra of the free-quark, ACCMM and GISW model are compared. The quark masses of the free-quark model used are: $m_b = 5.0\,GeV/c^2$ and $m_c = 1.7\,GeV/c^2$. The parameters taken for the ACCMM model are the fit results from Chapter 3. The similarity of the inclusive lepton spectra explains the slight differences in the semileptonic branching ratio found with the different theoretical models in Chapter 3.

Chapter 2

Experiment

2.1 Υ Resonances

The Υ resonances are bound states of a b and $\bar{b}$ quark with spin 1. They can be produced in e^+e^- annihilations via a virtual photon. Figure 2.1 shows the cross section of the four lowest mass Υ resonances in e^+e^- collisions as a function of center of mass energy measured at the Cornell electron storage ring (CESR) [12].

The $\Upsilon(4S)$ resonance is the lowest mass Υ resonance which can decay into a pair of B mesons. It is assumed that the $\Upsilon(4S)$ resonance decays 50 % of the time into neutral and 50 % into charged pairs of B mesons. The visible hadronic cross section of the $\Upsilon(4S)$ resonance is $\sigma = (0.85 \pm 0.04)\,nb$ at the DORIS II ring.

All Υ resonances lie on top of a continuum. The continuum processes contain all possible QED processes like production of $d\bar{d}$, $u\bar{u}$, $s\bar{s}$, $c\bar{c}$ quark pairs, e^+e^-, $\mu^+\mu^-$, $\tau^+\tau^-$ pairs, and $\gamma\gamma$ events.

For measurements of B decays the continuum under the $\Upsilon(4S)$ resonance has to be subtracted. This is done by taking data not only on the $\Upsilon(4S)$ resonance but also in the continuum below and subtracting the two data samples.

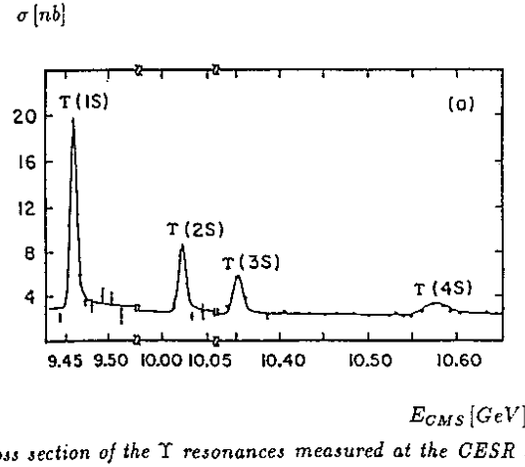

Figure 2.1: *Cross section of the Υ resonances measured at the CESR storage ring in Cornell* [12].

2.2 ARGUS Detector

The ARGUS detector, shown in Figure 2.2, was designed as a universal tool to investigate final states from e^+e^- annihilation processes. ARGUS started operation in October 1982 and has since successfully taken data at the $\Upsilon(1S)$, $\Upsilon(2S)$ and $\Upsilon(4S)$ energies and in the nearby continuum.

2.2.1 Detector Components

A particle originating from the interaction region and leaving the beam tube traverses the following components: the vertex chamber, the main drift chamber, the time-of-flight system, and the calorimeter. Muons passing through the magnet coils and flux return yoke hit the muon chambers surrounding the detector.

The drift chamber is the central component of the detector and has a twofold purpose. It serves as a track detector and as a device to identify charged particles measuring their momenta and specific energy losses due to the ionization of the chamber gas. The vertex chamber considerably improves the accuracy of the measurement of the track parameters and vertices.

The main purpose of the time-of-flight system is to determine the velocities of charged particles by measuring their flight time. Using the momenta measured in the drift chamber, one can identify particles by their rest mass.

The electromagnetic calorimeter fulfills two tasks. It measures the energy of photons and neutral particles, and it supports discrimination between electrons and hadrons.

The muon system completes the ARGUS particle detection capability. It covers about 90 % of the solid angle.

The resolutions of the detector components are best in the barrel region where the lepton spectra of Chapter 3 are measured. The resolution of each component is listed in Table 2.2.1.

Component	Property	Resolution
ToF Counter	Time	$220\,ps$
Drift Chamber	dE/dx	4.5 % – 5.5 %
Shower Counter	Energy	$(0.072^2 + 0.065^2/E[GeV])^{1/2}$
Drift + Vertex Chamber	Momentum	$(0.01^2 + (0.006 p_T[GeV/c])^2)^{1/2}$

Table 2.1: *Resolution of the ARGUS detector components in the barrel region* [3].

2.2.2 Particle Identification

ARGUS provides two independent methods for charged particle identification, namely, the measurement of the specific energy loss in the drift chamber and the measurement of the time-of-fight. Together with the momentum measurement in the drift chamber, they enable to reconstruct a particle's mass.

A comparison of a particles dE/dx measured in the drift chamber with theoretical expectations results in a χ^2 for each particle hypothesis:

$$\chi_i^2(dE/dx) = \frac{(dE/dx - dE/dx_i^{th})^2}{\sigma_{dE/dx}^2 + \sigma_{th}^2} \; ; \quad i = (e,\, \mu,\, \pi,\, K,\, p) \tag{2.1}$$

where dE/dx_i^{th} is the specific ionization loss expected theoretically for the ith particle hypothesis, σ_{th} the uncertainty in the theoretical dE/dx value, and $\sigma_{dE/dx}$ the uncertainty in the specific ionization measurement.

A similar procedure is used for the ToF information by comparing the measured velocity with that expected for the above mentioned particle hypothesis. This results in a χ^2 of the form:

$$\chi_i^2(ToF) = \frac{(1/\beta - 1/\beta_i^{th})^2}{\sigma_{ToF}^2 + \sigma_{th}^2} \tag{2.2}$$

where β is the particles velocity measured by the time-of-flight system, β_i^{th} the velocity expected for the ith particle hypothesis, and σ_{ToF} and σ_{th} are the uncertainties of the measured and expected velocities.

Since the dE/dx and ToF are independent the χ^2 can be added:

$$\chi_i^2 = \chi_i^2(dE/dx) + \chi_i^2(ToF)\,. \tag{2.3}$$

From the χ^2 normalized likelihoods LH_i are constructed:

$$LH_i^{dE/dx,\,ToF} = \frac{w_i e^{-\chi_i^2/2}}{\sum_j w_j e^{-\chi_j^2/2}} \; ; \quad i,\, j = (e,\, \mu,\, \pi,\, K,\, p) \tag{2.4}$$

where the w_i are relative production rates introduced from an a priori knowledge of the particle abundances.

For lepton identification there are, in addition, independent methods. Electrons can be identified by the means of dE/dx, ToF and shower counter information. The normalized likelihood reads:

$$\lambda_e = \frac{w^e \prod_{i=dE/dx,\,ToF,\,SC} p_i^e(x)}{\sum_{k=e,\,\mu,\,\pi,\,K,\,p} w^k \prod_{i=dE/dx,\,ToF,\,SC} p_i^k(x)} \tag{2.5}$$

where the $p_i^k(x)$ are the probabilities for a track with measured parameter x to be identified as particle type k by device i. Muon identification is based on dE/dx, ToF, shower counter and muon chamber measurements. Here, a further condition is that the track reconstructed in the drift chamber has to match with a hit in a muon chamber. The normalized likelihood reads:

$$\lambda_\mu = \frac{w^\mu \prod_{i=dE/dx,\,ToF,\,SC,\,\mu} p_i^\mu(x)}{\sum_{i=e,\,\mu,\,\pi,\,K,\,p} w^k \prod_{i=dE/dx,\,ToF,\,SC,\,\mu} p_i^k(x)}\,. \tag{2.6}$$

Photons are identified by a signal in the calorimeter and no matching signal in the drift and vertex chamber.

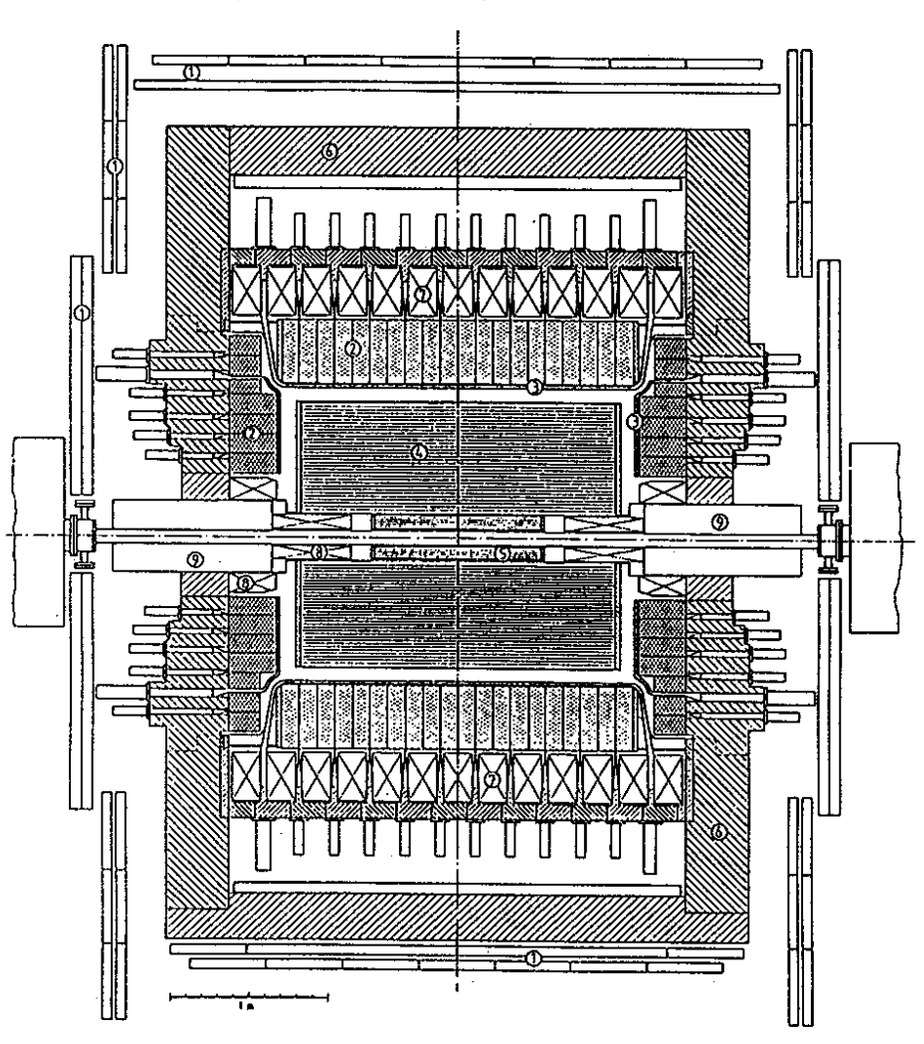

Figure 2.2: *The ARGUS detector (cut along the beam axis).*
1) muon chamber *2) calorimeter* *3) time-of-flight*
4) drift chamber *5) vertex chamber* *6) iron yoke*
7) magnet coil *8) compensation coils* *9) mini-β-quadrupoles*

Chapter 3

Model Dependent Inclusive Semileptonic Branching Ratio of B Mesons with Lepton Spectra

In order to determine the inclusive semileptonic branching ratio of B mesons, theoretical models are used to fit the lepton spectra from B decays. Therefore, the measured lepton spectra from the $\Upsilon(4S)$ resonance have to be corrected in a variety of ways. After subtracting contributions from the continuum and as lepton misidentified hadrons, the spectra are corrected for detector acceptances. Then a few leptonic backgrounds resulting from the B decays are subtracted.

After these corrections the lepton spectra consist of only three contributions: semileptonic $b \to c$, $c \to s$, and $b \to u$ quark transitions. In order to determine the amount of $b \to c$ transitions theoretical spectra describing the three remaining contributions from semileptonic quark transitions are fit to the corrected lepton spectra.

Dividing the efficiency corrected number of semileptonic $b \to c$ decays by the number of B mesons in the data sample gives the inclusive semileptonic branching ratio of B mesons. Out of this, the Cabibbo-Kobayashi-Maskawa matrix element $|V_{cb}|$ can be determined within every theoretical model which is fit to lepton spectra.

3.1 Cuts for Event and Lepton Selection

3.1.1 Event Selection

The event selection criteria are designed to enrich the data sample with $\Upsilon(4S)$ events, i.e. $B\bar{B}$ events. This is done by suppressing continuum events and events where beam electrons interact with gas molecules in the storage ring or beam pipe, the so called beam-gas and beam-wall events. Continuum, beam-gas, and beam-wall events have a smaller charged track multiplicity than $\Upsilon(4S)$ events. A cut on the number of charged tracks, N_{Ch}, of

$$N_{Ch} \geq 5 \tag{3.1}$$

suppresses these backgrounds efficiently without affecting the $B\bar{B}$ events. Tracks from converting photons, decaying K^0 and Λ^0 are not included in the number of charged tracks.

Beam-gas and beam-wall events should be suppressed as much as possible. They are normally accompanied by electrons and can not be subtracted like continuum events. The beam energy dependence of the cross section is not known and most probably different from the dependence exhibited by the continuum. In contrast to e^+e^- events, beam-gas and beam-wall events are distributed equally along the storage ring. Hence, they can be suppressed by requiring that charged tracks originate from a certain volume around the nominal interaction point:

$$r \leq 1.5\,cm \quad \text{and} \quad |z| \leq 5.0\,cm\,, \tag{3.2}$$

where r is the radial distance from the nominal interaction point perpendicular to beam axis and z the distance along the beam axis. In addition, tracks have to point to the main vertex within 10 standard deviations.

Due to the detector geometry, charged tracks can only be recognized in a region defined by polar angle θ:

$$\cos\theta \leq 0.92\,. \tag{3.3}$$

Converted photons are a source of electrons and positrons which should be rejected. An electron-positron pair is reconstructed as a converted photon if it has an invariant mass compatible with zero within the detector resolution, i.e. $m_{e^+e^-} \leq 50\,MeV/c^2$.

3.1.2 Lepton Selection

Leptons are selected according to criteria which observe both high detection efficiency and low misidentification rates. Electron identification is based mainly on comparison of the energy measured in the shower counters and the momentum measured in the drift chamber. The energy resolution of the calorimeter and the momentum resolution of the drift chamber are best in the barrel region. The polar angle θ of electron candidates with respect to the beam line is, therefore, restricted to:

$$|\cos\theta| < 0.7\,. \tag{3.4}$$

In order to simplify comparisons between muons and electrons, muon candidates must also satisfy this condition.

The likelihood functions λ_e and λ_μ for electrons and muons, respectively, have both to exceed a certain value. A cut at a value of

$$\lambda_{e,\mu} \geq 0.7 \tag{3.5}$$

leads to high efficiency in the lepton identification and small background due to hadrons misidentified as leptons.

Since muons are the only long-lived charged particles which can easily penetrate the calorimeter and iron coil, at least one hit in an outer muon chamber is required for muon candidates.

3.2 Time Integrated Luminosity and Number of B Mesons

In order to measure the branching ratio of inclusive semileptonic B decays, not only the number of leptons from semileptonic B decays is needed, the number of B mesons

in the data sample is needed as well. This number is calculated from the number of multi hadron events collected on the $\Upsilon(4S)$ resonance and in the nearby continuum. Applications of the event selection cuts of Section 3.1.1 leads to the number of multi hadrons and time integrated luminosities listed in Table 3.1.

	$\Upsilon(4S)$	Continuum
$\sqrt{s}\,[GeV]$	10.58	10.46
$\mathcal{L}\,[pb^{-1}]$	218	83
N_{Muha}	740267	220369

Table 3.1: *Time integrated luminosity and number of multi hadron events at different center of mass energies.*

The cross section for QED processes is inversely proportional to the square of the center of mass energy. Therefore, the number of events from the $\Upsilon(4S)$ resonance $N_{\Upsilon(4S)}$ in the data sample can be calculated with:

$$N_{\Upsilon(4S)} = (N_{on} - \frac{\mathcal{L}_{on}}{\mathcal{L}_{off}} \frac{s_{off}}{s_{on}} N_{off})/\epsilon \qquad (3.6)$$

where N_i, s_i and $\mathcal{L}_i$ are, respectively, the number of multi hadron events, the squared center of mass energies, and the time integrated luminosities. The probability for an event to pass the selection criteria ϵ is determined with Monte Carlo.

If one assumes that the $\Upsilon(4S)$ resonance decays 100 % of the time into $B\bar{B}$ pairs, the number of B mesons in the data is [7]:

$$N_B = 368800 \pm 15600\,. \qquad (3.7)$$

3.3 Measurement of Lepton Spectra

Applying the above mentioned selection criteria leads to the electron spectrum shown in Figure 3.1 and the muon spectrum shown in Figure 3.2. The momentum spectra contain leptons from

- semileptonic B decays, semileptonic D Decays,
- continuum,
- hadrons misidentified as leptons (fakes) and
- leptons from the decay chain of B mesons which do not come from semileptonic B or D decays.

These lepton spectra must be corrected so that they reflect the spectra of leptons from semileptonic B and D meson decays alone. This means the last three contributions above have to be subtracted.

The continuum contribution is subtracted with continuum data measured below the $\Upsilon(4S)$ resonance. Fakes are subtracted by determining the fake lepton rate with $\Upsilon(1S)$ data and multiplying it with the hadron spectrum from $\Upsilon(4S)$ data. Leptons

which are produced by decays of J/ψ, τ and Λ_c from B decays are subtracted by Monte Carlo generated spectra scaled by the branching ratios found in [31]. Leptons remaining from converted photons are taken into account by a full simulation of the detector [29,36].

The resulting lepton spectra are fit with theoretical descriptions of semileptonic $b \to c$, $b \to u$, and $c \to s$ quark decays. Four different models for the $b \to c$ transitions are used: the free-quark, the ACCMM, the GISW and a modified version of the GISW model with free D^{**} content.

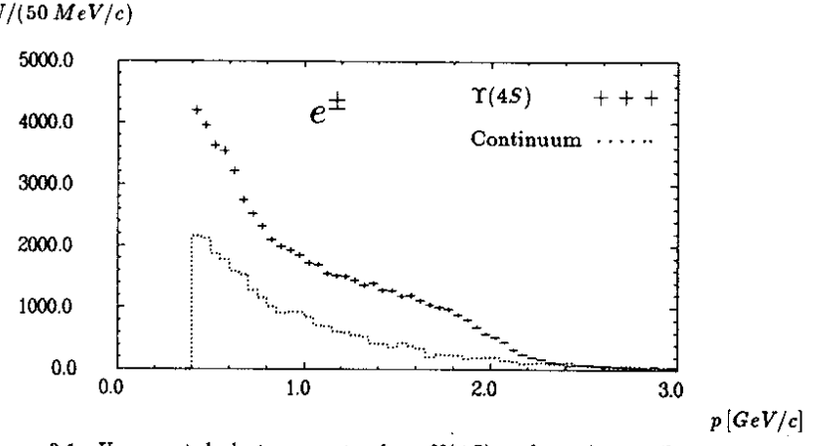

Figure 3.1: *Uncorrected electron spectra from $\Upsilon(4S)$ and continuum (luminosity and momentum scaled).*

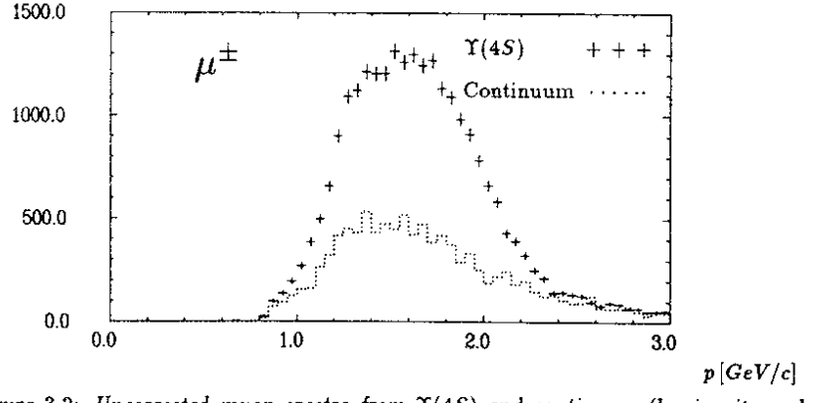

Figure 3.2: *Uncorrected muon spectra from $\Upsilon(4S)$ and continuum (luminosity and momentum scaled).*

3.3.1 Continuum Subtraction

The continuum contribution at the $\Upsilon(4S)$ resonance is subtracted using continuum data recorded below the $\Upsilon(4S)$ (see Figure 2.1). The number of events in the continuum is scaled according to the measured time integrated luminosity on the $\Upsilon(4S)$ resonance $\mathcal{L}_{on}$ and the continuum $\mathcal{L}_{off}$ and their squared center of mass energies s_{on} and s_{off}. The continuum scaling factor r is:

$$r = \frac{\mathcal{L}_{on}}{\mathcal{L}_{off}} \frac{s_{off}}{s_{on}} = 2.58 \pm 0.03 \,. \tag{3.8}$$

Because the center of mass energies in the $\Upsilon(4S)$ data and the continuum data are different, the momentum of the tracks measured in the continuum are scaled linearly with the beam energy:

$$p' = p \frac{\sqrt{s_{on}}}{\sqrt{s_{off}}} \,. \tag{3.9}$$

The luminosity and momentum scaled continua for electrons and muons can be seen in Figure 3.1 and in Figure 3.2. The direct, i.e. continuum subtracted, lepton spectra from the $\Upsilon(4S)$ resonance are shown in Figure 3.3 and in Figure 3.4.

3.3.2 Fake Subtraction

Hadrons can be misidentified as electrons and muons. Therefore, it is necessary to subtract these faked leptons from the lepton spectra.

In order to determine the fake rate, a lepton free data sample has to be found. The lepton selection criteria used to extract the lepton spectra from the $\Upsilon(4S)$ resonance and the continuum are applied to the sample to determine how often hadrons are misidentified as leptons.

A lepton free data sample can be collected on the $\Upsilon(1S)$ resonance. The $\Upsilon(1S)$ resonance decays predominantly via three gluons into hadrons. Only upper limits are known [5] for charm production from $\Upsilon(1S)$ decays.

One advantage of determining the fake rate with $\Upsilon(1S)$ data is the similarity of $\Upsilon(1S)$ and $\Upsilon(4S)$ event topologies. Another advantage is the large sample of $\Upsilon(1S)$ data collected by the ARGUS experiment.

After continuum subtraction in the $\Upsilon(1S)$ data, the fake rates η_e and η_μ for electrons and muons, respectively, are:

$$\eta_e = \frac{\text{all tracks with } \lambda_e > 0.7}{\text{all tracks}} \,, \tag{3.10}$$

$$\eta_\mu = \frac{\text{all tracks with } \lambda_\mu > 0.7 \text{ and at least one hit in an outer } \mu \text{ chamber}}{\text{all tracks}} \,. \tag{3.11}$$

The tracks are confined to the barrel region of the ARGUS detector like in the measurement of lepton spectra of the $\Upsilon(4S)$ resonance.

Multiplying the fake rate spectrum of the $\Upsilon(1S)$ data with the continuum subtracted hadron spectrum of the $\Upsilon(4S)$ resonance gives the fake spectrum of $\Upsilon(4S)$.

In order to determine the hadron spectrum of the $\Upsilon(4S)$ resonance and the continuum, the lepton selection criteria are inverted. A track is taken as a hadron if:

$$(\lambda_e < 0.7) \text{ and } ([\lambda_\mu < 0.7] \text{ or } [\text{no hit in an outer } \mu \text{ chamber}]) \,. \tag{3.12}$$

The fake spectra for electrons and muons can be seen in Figure 3.3 and 3.4 together with the continuum subtracted lepton spectra on the $\Upsilon(4S)$ resonance.

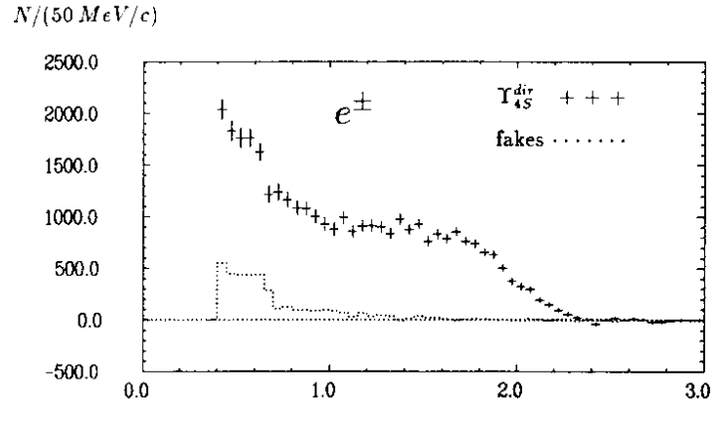

Figure 3.3: *Continuum subtracted electron spectrum on $\Upsilon(4S)$ and fake electron spectrum.*

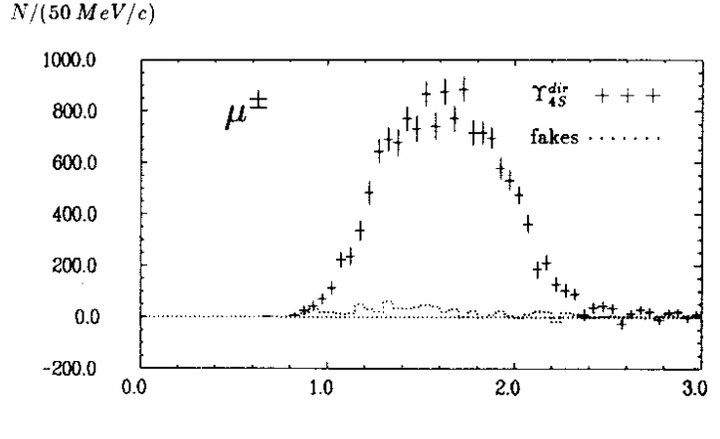

Figure 3.4: *Continuum subtracted muon spectrum on $\Upsilon(4S)$ and fake muon spectrum.*

3.3.3 Efficiency Correction

The number of found leptons and events has to be corrected in many ways for acceptance losses. The efficiencies of the likelihood functions for electron and muon recognition are corrected for with a data sample consisting only of electrons and muons. The acceptance for the event selection, trigger, vertex fit and track reconstruction probability are determined through Monte Carlo simulation.

Efficiency Correction to the Electron Likelihood λ_e

Bhabha events provide a data sample which consists only of electrons and positrons. It can be used to determine the efficiency of the likelihood function λ_e has for recognizing electrons. Radiative Bhabha events, i.e. Bhabha events which radiate a photon, provide a means for determining the momentum dependence of this acceptance.

The radiative Bhabha candidates can not be selected using the likelihood function λ_e which has to be tested. They are only selected with kinematic cuts:

The event must have exactly two charged tracks pointing to the interaction region with opposite charge. The energy of the photon has to exceed a limit of:

$$E_\gamma \geq 1\,GeV \tag{3.13}$$

The tracks are restricted to a region where the leptons of the spectra are measured, the barrel region of the ARGUS detector:

$$|\cos\theta| \leq 0.7\,. \tag{3.14}$$

The energy of the two charged tracks plus the photon measured by the calorimeter should be equal within $0.5\,GeV$ to the center of mass energy:

$$|E_{sum} - \sqrt{s}| \leq 0.5\,GeV\,. \tag{3.15}$$

The total transverse momentum p_{trans} of the event should be consistent with zero:

$$p_{trans} \leq 0.3\,GeV/c\,. \tag{3.16}$$

The tracks of the event should not overlap in the detector. The momentum vectors of the $e^\pm$ candidates $\vec{p_e}$ and the γ candidate $\vec{p_\gamma}$ have to fulfill:

$$(\vec{p_e},\vec{p_\gamma}) \geq 30^\circ \text{ and } (\vec{p_e},\vec{p_e}) \geq 45^\circ\,. \tag{3.17}$$

After applying the above cuts, the momentum-dependent efficiency ϵ_e of the likelihood function λ_e is determined by:

$$\epsilon_e = \frac{\text{tracks with } \lambda_e > 0.7}{\text{all tracks}}\,. \tag{3.18}$$

Since the track multiplicity of $\Upsilon(4S)$ events is greater than that of the selected Bhabha candidates, electrons can overlap with other tracks in $\Upsilon(4S)$ events. The resulting efficiency losses of the electron likelihood function λ_e and the muon likelihood function λ_μ are calculated with Monte Carlo and found to be $(2.4 \pm 0.9)\,\%$.

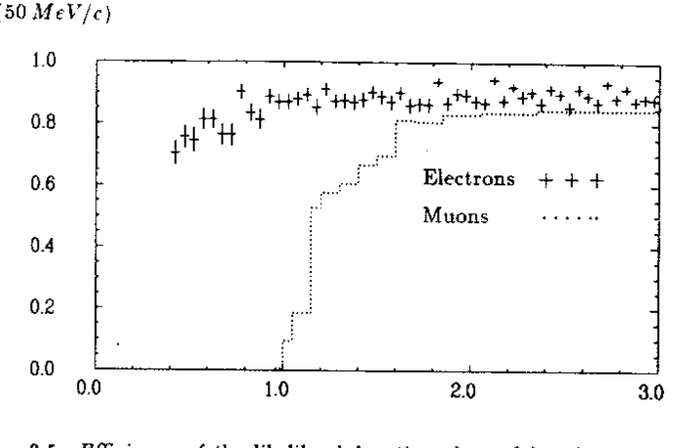

Figure 3.5: *Efficiency of the likelihood functions λ_e and λ_μ. λ_e is determined with radiative Bhabha pairs, λ_μ with MC* [36].

Efficiency Correction to the Muon Likelihood λ_μ

The cross section of radiative muon pairs is because of the muon mass much smaller than the one of radiative Bhabha pairs. A data sample with enough events to measure the efficiency of the muon likelihood function λ_μ is not available. Therefore, the muon likelihood function efficiency ϵ_μ is determined with Monte Carlo simulation [36]. The muon tracking in the ARGUS simulation program is tuned with cosmic rays [19].

The acceptances of the electron and muon likelihood functions λ_e and λ_μ are shown in Figure 3.5. λ_μ falls down to zero below $1\,GeV/c$ because slow muons can not penetrate the iron yoke of the ARGUS detector and hit the outer muon chambers.

Further Efficiencies

There are further efficiencies which have to be taken into account to determine the number of semileptonic B meson decays. Except for the efficiency of the angular cut of $|\cos\theta| < 0.7$, they are all estimated by Monte Carlo simulation [29,36]. These efficiencies are the following: the efficiency for an event with a semileptonic B decay to pass the event selection criteria ϵ_{SL}, to be triggered by the data aquisition system, and to have its lepton track be reconstructed and fit to the main vertex. The efficiencies are listed in Table 3.2.

Efficiency	e	μ
$\lvert\cos\theta\rvert \leq 0.7$	0.70 ± 0.00	0.70 ± 0.00
ϵ_{SL}	0.92 ± 0.01	0.92 ± 0.01
Trigger	1.00 ± 0.01	1.00 ± 0.01
VX Fit + Track Reco	0.98 ± 0.01	0.99 ± 0.01
Π	0.63 ± 0.01	0.64 ± 0.01

Table 3.2: *MC* [29,36] *determined efficiencies (see explanations in text).*

3.3.4 Subtraction of Backgrounds Resulting from B Decays

There are four backgrounds of leptons arising from B meson decays which are not semileptonic B or D meson decays. These are leptonic decays of J/ψ mesons, τ leptons, and semileptonic decays of Λ_c baryons, and converted photons produced in B decays.

The production rates of J/ψ, τ and Λ_c and their branching ratios to leptons are taken from [26,31,38]:

Background	Branching Ratio [%]
$B \to XJ/\Psi$	1.12 ± 0.16
$J/\Psi \to l^+l^-$	6.15 ± 0.16
$B \to X\tau^-$	2.9 ± 1.9
$\tau^- \to l^-\nu_l\bar{\nu}_\tau$	17.76 ± 0.19
$B \to X\Lambda_c$	7.5 ± 1.9
$\Lambda_c^- \to Xl^-\bar{\nu}_l$	4.5 ± 1.7

Table 3.3: *Backgrounds from B decays which are not from semileptonic B or D decays.*

Converted photons are also a source of electrons and positrons. Although a cut against converted photons is applied at the event selection a few of them still contribute to the lepton spectra. This results from unreconstructed electron or positron tracks. The remaining electrons and positrons from converted photons are subtracted from the lepton spectra of the $\Upsilon(4S)$ resonance with a full detector simulation of B meson decays [29,36].

The electron spectra from J/ψ, τ, Λ_c decays and the converted photons can be seen in Figure 3.6 to 3.9. They are normalized to the branching ratios in Table 3.3 and efficiencies in Table 3.2.

3.3.5 Number of Electrons and Muons

The number of electrons and muons found on the $\Upsilon(4S)$ resonance and the various backgrounds are listed in Table 3.4. For the electrons the momentum interval $[0.4\,GeV/c, 3.0\,GeV/c]$ is used and $[1.3\,GeV/c, 3.0\,GeV/c]$ for the muons.

Number of Leptons	e	μ
$\Upsilon(4S)$	61021 ± 247	20080 ± 142
Continuum	10571 ± 103	3138 ± 56
Fakes	3663 ± 516	461 ± 70
$B \to X\tau^- \to l^-\nu\bar{\nu}$	910 ± 703	90 ± 62
$B \to X\Lambda_c \to Xl^-\bar{\nu}$	534 ± 238	3 ± 1
$B \to XJ/\psi \to l^+l^-$	350 ± 72	291 ± 66
$B \to X\gamma \to e^+e^-$	140 ± 12	–

Table 3.4: *Number of leptons on $\Upsilon(4S)$ and backgrounds.*

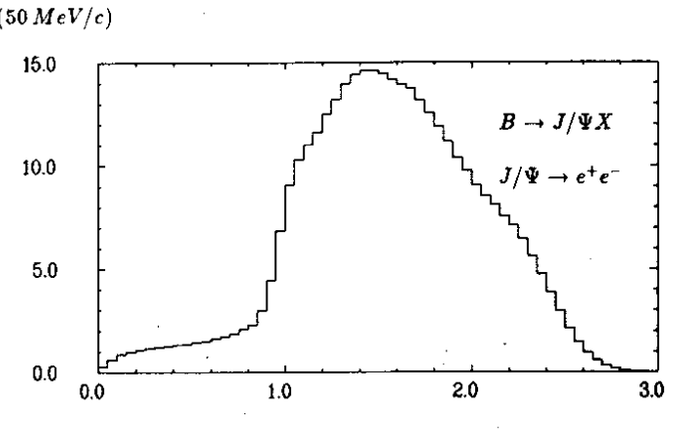

Figure 3.6: *Monte Carlo simulated electron spectrum of the decay $B \to XJ/\Psi$, $J/\Psi \to e^+e^-$.*

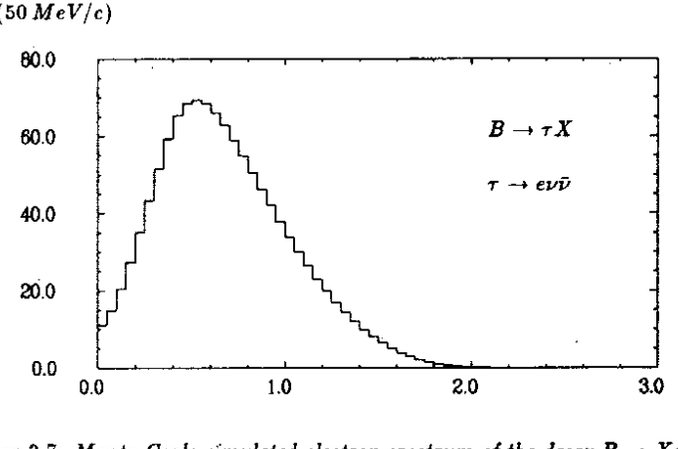

Figure 3.7: *Monte Carlo simulated electron spectrum of the decay $B \to X\tau$, $\tau \to e\nu\bar{\nu}$.*

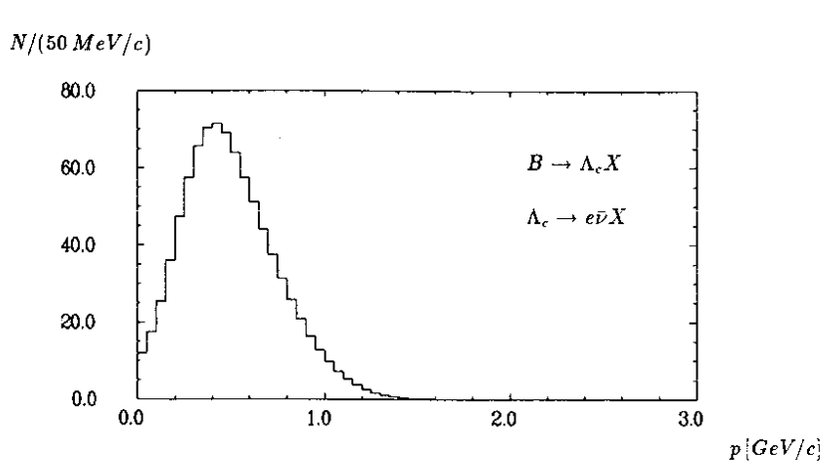

Figure 3.8: *Monte Carlo simulated electron spectrum of the decay* $B \to X\Lambda_c$, $\Lambda_c \to Xe\bar{\nu}$.

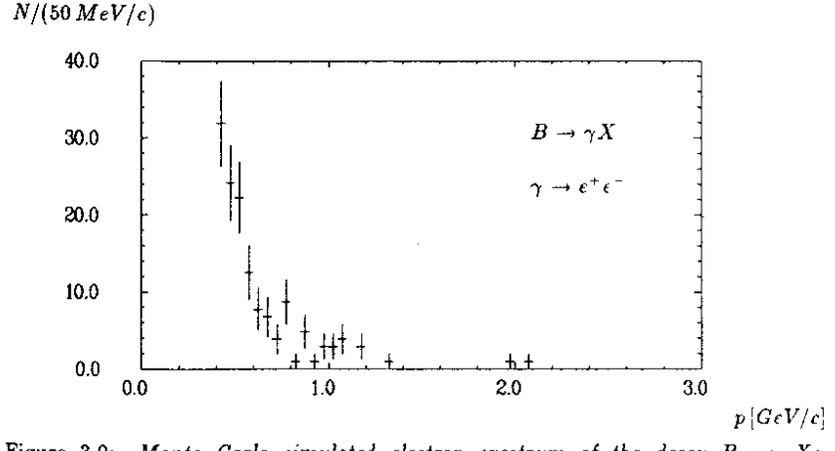

Figure 3.9: *Monte Carlo simulated electron spectrum of the decay* $B \to X\gamma$, $\gamma \to e^+e^-$.

3.3.6 Systematic Errors on the Inclusive Semileptonic Branching Ratio of B Mesons

Special attention has to be given to the systematic error of this measurement. It will turn out in Section 3.4, where the fits of the theoretical models to lepton spectra are performed, that the systematic uncertainties are greater than the statistical ones. All sources of systematic uncertainty are briefly described here, along with how their values are determined. The numerical contribution of each systematic error is listed in Table 3.5.

Relative Contribution to Systematic Error on $BR(B \to Xl\nu)$ in %	e	μ
Number of B mesons	4.4	4.4
Lepton Identification Eff.	2.8	4.2
Fakes	0.2	0.9
Track and Vertex Rec. Eff.	0.9	1.1
Trigger Efficiency	1.3	1.2
ϵ_{SL}	0.9	0.8
$b \to u$ Model	0.0	0.0
$c \to s$ Model	0.3	0.3
$B \to J/\psi X$	0.3	0.3
$B \to \tau X$	1.5	1.5
$B \to \Lambda_c X$	0.2	0.2
$B \to \gamma X$	0.0	–
Bremsstrahlung	0.7	–
$\sum$ (in Quadrature)	5.8	6.6

Table 3.5: *Relative systematic errors on the inclusive semileptonic branching ratio of* B *mesons in %.*

The dominant systematic uncertainty in this measurement is the error on the number of B mesons of 4.4%. This error is dominated by the uncertainty in the luminosity ratio of $\Upsilon(4S)$ and continuum data of 1.7% [7].

The systematic error due to fake subtraction is determined by using fake rates from two different methods: examining $\Upsilon(1S)$ data and investigating reconstructed particles in $\Upsilon(4S)$ data. Λ baryons, K^0 and Φ mesons are reconstructed in order to get particle specific fake rates for π^+, K^+ mesons, and (anti) protons. The fake rates are weighted according to particle abundance and summed. The difference in the yielded fake rates with these two methods is considered to be the systematic error of the fake rate. In the case of electrons, the free amount of semileptonic D meson decays can compensate for fake rate differences in the fits to the measured lepton spectra (see Section 3.4).

The systematic uncertainty of the electron identification is obtained in a similar way. In the case of electrons, the tracks of Bhabha events are selected with different methods: with and without application of electron identification to the track not used in the efficiency determination. The lepton identification efficiency is also compared with the result from the Monte Carlo simulation. The variation in the semileptonic

branching ratios obtained using the three methods is taken as the systematic error in the lepton identification efficiency. It reaches the precision of $(2-3)\,\%$ described in [39]. In the case of muons, there is only one way to determine the identification efficiency, i.e. the Monte Carlo Method. Therefore, one and a half of the systematic error of the electron identification is taken as an estimation for the error of the muon identification. The MC muon identification efficiency is tuned with cosmic rays [19,36].

The systematic error in the efficiency of the selection of semileptonic B decays is determined with Monte Carlo. The event selection criteria are slightly changed, for example four instead of five charged tracks are required for the event selection. The variation of the semileptonic branching ratio of B mesons in the Monte Carlo gives the systematic error in the efficiency of the selection of semileptonic B decays.

The error in the model dependence of semileptonic $b \to u$ and $c \to s$ spectra is estimated by using different theoretical models.

The determination of the systematic error contributions from J/ψ mesons, Λ_c baryons, and τ leptons resulting from B decays is straight forward. The uncertainties in their production rates and their leptonic branching ratios are varied by one standard deviation. The variation in the semileptonic branching ratio of B mesons is taken as the systematic error. The systematic error on the number of remaining electron and positron tracks from converted photons after the cut against them is assumed to be equal to the systematic error on the contribution from τ leptons from B decays.

For electron spectra produced by Monte Carlo, bremsstrahlung effects have to be applied. Different amounts of detector material change the shape of the electron spectra. This is especially important for the primary spectra from semileptonic B decays. The smaller the background contribution, the less important this effect becomes. The amount of detector material was varied in each direction by 10 % to find out the systematic error on the bremsstrahlung effects.

The error on the track and vertex reconstruction efficiency is estimated from the χ^2 distribution of the vertices like in [11].

3.3.7 Systematic Errors on $|V_{cb}|$

The systematic errors on the Cabibbo-Kobayashi-Maskawa matrix element $|V_{cb}|$ have to be divided into experimental and theoretical ones.

The errors due to the measurement of the semileptonic branching ratio and the lifetime have to be taken into account in all models. Their relative values are 2.5 % and 1.9 % of $|V_{cb}|$ for the branching ratio and the lifetime, respectively.

Relative Contribution to Error on $\lvert V_{cb}\rvert$ in %	e	μ	$\frac{e+\mu}{2}$
BR	2.5	2.5	2.5
τ_B	1.9	1.9	1.9
m_b	5.1	6.0	3.7
m_c	2.2	3.5	2.6

Table 3.6: *Relative contributions to error on $|V_{cb}|$ of Free-Quark and ACCMM model.*

The theoretical errors on $|V_{cb}|$ in the free-quark and ACCMM model arise from the uncertainty in the quark masses. Since the endpoint of the lepton momentum spectrum is given by the quark mass differences of the decaying and final state quark, the masses are correlated. The errors on the quark masses have, therefore, to be added linearly. For the free-quark model, the errors of the ACCMM model are used to determine the contribution to the error on $|V_{cb}|$. The different relative error contributions of the Kobayashi-Maskawa matrix element V_{cb} are summarized in Table 3.6.

The relative theoretical uncertainty in the GISW model is quoted to be 12.5 % [20]. According to the authors, this is mainly due to the uncertainty in the choice of the wave functions.

3.4 Fits to Corrected Lepton Spectra

This Section describes how the theoretical models are fit to the measured and corrected lepton spectra. The resulting values for the inclusive semileptonic branching ratio and Cabibbo-Kobayashi-Maskawa matrix element $|V_{cb}|$ are given for each theoretical model used.

At this point, the lepton spectra of the $\Upsilon(4S)$ resonance have been corrected for continuum contributions, fakes, and leptons from J/ψ, Λ_c, τ decays, converted photons from B decays, and detection efficiency. Hence, the corrected lepton spectra consist only of three contributions: semileptonic $b \to c$, $b \to u$, and $c \to s$ quark transitions.

With a simultaneous fit of the theoretical lepton spectra of these three quark transitions to the measured spectra, the contribution from each can be determined. The experimental spectra are, therefore, described by the following sum:

$$\left(\frac{dN}{dp}\right)^{exp} = a\left(\frac{dN}{dp}\right)^{b\to c} + b\left(\frac{dN}{dp}\right)^{c\to s} + c\left(\frac{dN}{dp}\right)^{b\to u} \qquad (3.19)$$

where a, b, and c reflect the proportions of the semileptonic quark transitions and the various dN/dp symbolize the momentum spectra.

The contribution which yields together with number of B mesons the inclusive semileptonic branching ratio of B decays is the $b \to c$ component. This is described with four different models: the free-quark, ACCMM, GISW, and a modified GISW model.

For semileptonic $c \to s$ decays, the ACCMM model is used. The s quark mass is set to $m_s = 0.3\,GeV/c^2$, the spectator quark mass to $m_{sp} = 0.15\,GeV/c^2$, and the Fermi momentum to $p_F = 0.15\,GeV/c$, as suggested by [1].

Semileptonic $b \to u$ transitions are only a small component of the lepton spectrum. Their contribution is fixed using $|V_{ub}|/|V_{cb}| = 0.1$, as measured by [9]. Phase space factors f_{qb} and gluon corrections factors g_{qb} are taken from [10]:

$$\frac{f_{ub}}{f_{cb}}\frac{g_{ub}}{g_{cb}} = 1.8\,. \qquad (3.20)$$

This would correspond to an inclusive semileptonic branching ratio for $b \to u$ decays of 0.18 % if the inclusive semileptonic branching ratio of $b \to c$ decays were 10 %. The lepton spectrum is taken from the ACCMM model with a u quark mass $m_u = 0.15\,GeV/c^2$ and spectator quark mass $m_{sp} = 0.15\,GeV/c^2$.

When the electron spectrum is fit alone or simultaneously with the muon spectrum the contribution from $c \to s$ transitions is left a free parameter of the fit. In fits to the muon spectrum alone, the $c \to s$ component is held to the value obtained in the electron fits. The electron spectrum is fit from $0.4\,GeV/c$ to $3.0\,GeV/c$, the muon spectrum from $1.3\,GeV/c$ to $3.0\,GeV/c$.

Since the theoretical lepton spectra are predicted in the rest frame of the decaying meson, the spectra have to be boosted into the laboratory system. This is done with a Monte Carlo technique. In addition the lepton spectra are folded with the detector momentum resolution. In the case of electrons, bremsstrahlung corrections for both final state interactions and interactions with the detector material are applied as well.

The fits are carried out minimizing the following χ^2 function:

$$\chi^2 = \sum_i \frac{\left[\left(\frac{dN_i}{dp}\right)^{exp} - a\left(\frac{dN_i}{dp}\right)^{b\to c} - b\left(\frac{dN_i}{dp}\right)^{c\to s} - c\left(\frac{dN_i}{dp}\right)^{b\to u}\right]^2}{\left[\sigma\left(\frac{dN_i}{dp}\right)^{exp}\right]^2} \qquad (3.21)$$

where $\sigma\left(\frac{dN_i}{dp}\right)^{exp}$ is the error of the measured spectrum in each momentum bin, i.

3.4.1 Free-Quark Model

The first model fit to the lepton spectra is the free-quark model. The masses used for the b and c quarks are the fit results from the ACCMM model (see Section 3.4.2): $m_b = 5.0\,GeV/c^2$ and $m_c = 1.7\,GeV/c^2$.

The free-quark model gives the smallest inclusive semileptonic branching ratio for B mesons of all the fit models. Values range from $(9.4 \pm 0.6)\,\%$ for the muon spectrum fit to $(9.5 \pm 0.6)\,\%$ for the electron spectrum fit. The detailed numerical results of the fits can be found in Table 3.7. The first quoted error on the branching ratio is statistical, the second systematic. The fits to the corrected electron and muon spectra are shown in Figures 3.10 and 3.11, respectively.

Free-Quark Model	e	μ	$\frac{e+\mu}{2}$
$BR\,[\%]$	$9.5 \pm 0.2 \pm 0.6$	$9.4 \pm 0.2 \pm 0.6$	$9.4 \pm 0.1 \pm 0.6$
$\lvert V_{cb}\rvert \cdot 10^2$	$4.1 \pm 0.1 \pm 0.3$	$4.1 \pm 0.1 \pm 0.3$	$4.1 \pm 0.1 \pm 0.2$
χ^2/DoF	58.1/50	45.1/33	103.3/84

Table 3.7: *Results of fits to lepton spectra with the free-quark model.*

The mean value of the Cabibbo-Kobayashi-Maskawa matrix element $|V_{cb}|$ is in all three fits 0.041. It is not attached by the small branching ratio differences because it is only square root dependent on the inclusive semileptonic branching ratio. The first quoted error on $|V_{cb}|$ is the experimental error of this measurement combined with the B lifetime. The second error on $|V_{cb}|$ reflects the uncertainty in the quark masses used in the model.

Quark Mass Dependence of the Semileptonic Branching Ratio and $|V_{cb}|$

All theoretical models commonly applied to fit inclusive lepton spectra use different values of the b and c quark mass. Table 3.8 summarizes the changes in the semileptonic branching ratio and $|V_{cb}|$ with different quark masses. The b and c quark masses as well as their differences are varied according to the spread of the masses quoted in the models of [8,20,27] and found with the ACCMM model in the next Section.

The semileptonic branching ratio and $|V_{cb}|$ change only slightly as long as the differences in the b and c quark masses are constant (see upper part of Table 3.8). The best fits are obtained with a quark mass difference of $3.3\,GeV/c^2$, the mass difference obtained with the ACCMM and quoted in the GISW model. The changes in the branching ratio and $|V_{cb}|$ are more severe if the b quark mass is varied and the c quark mass held constant and vice versa (see middle and lower part of Table 3.8). A quark mass difference unequal with $3.3\,GeV/c^2$ leads to large χ^2 values of the fit.

$BR\,[\%]$	$\lvert V_{cb}\rvert \cdot 10^2$	χ^2	$m_b\,[GeV/c^2]$	$m_c\,[GeV/c^2]$
9.5	4.2	108	4.9	1.6
9.4	4.1	103	5.0	1.7
9.4	4.0	108	5.1	1.8
9.8	4.5	166	4.9	1.7
9.4	4.1	103	5.0	1.7
8.9	3.7	196	5.1	1.7
9.8	4.4	137	5.0	1.8
9.4	4.1	103	5.0	1.7
9.0	3.8	164	5.0	1.6

Table 3.8: *Quark mass dependence of the semileptonic branching ratio and $|V_{cb}|$ in the free-quark model. Electrons and muons are fit simultaneously. The number of degrees of freedom is 84.*

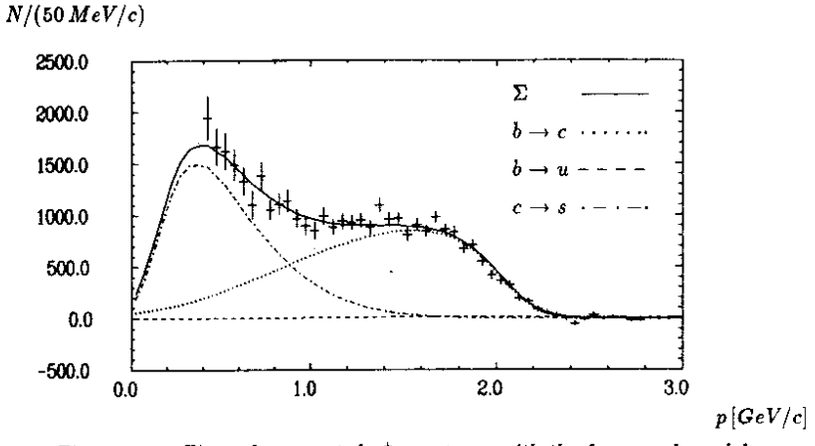

Figure 3.10: *Fit to the corrected $e^{\pm}$ spectrum with the free-quark model.*

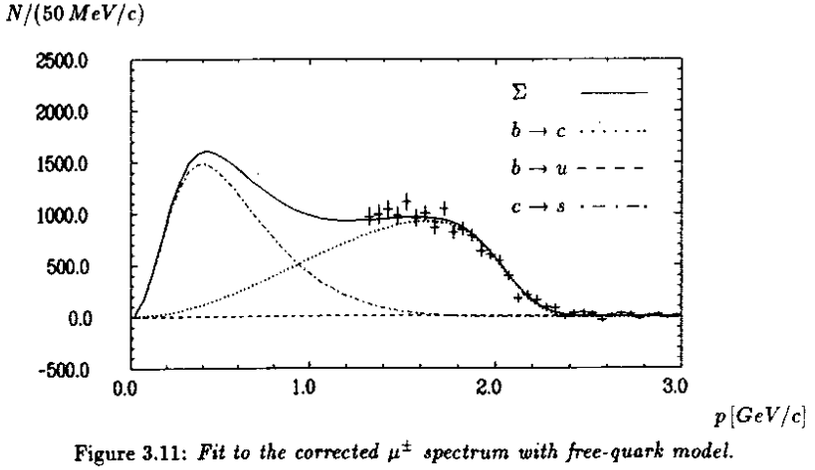

Figure 3.11: *Fit to the corrected $\mu^{\pm}$ spectrum with free-quark model.*

3.4.2 ACCMM Model

The second model fit to the lepton spectra is the ACCMM model. In the fits with the ACCMM model there are two additional free parameters for describing the lepton spectrum of $b \to c$ decays: p_F and m_c. The mass of the B meson spectator quark is fixed to $m_{sp} = 0.15\,GeV/c^2$ (see Section 1.1.2).

The results of the fits separately and simultaneously can be found in Table 3.9. The fits to the electron and muon spectra are shown in Figures 3.12 and 3.13, respectively.

The ACCMM model gives the largest semileptonic branching ratios compared to the other models employed in this work. Values range from $(9.7 \pm 0.2 \pm 0.6)\,\%$ for the electron fit and combined electron-muon fit to $(9.8 \pm 0.3 \pm 0.6)\,\%$ for the muon fit. The statistical errors are slightly greater than those of the free-quark model because of the two additional fit parameters of the ACCMM model.

The c quark mass values resulting from the electron and muon fits display a discrepancy of slightly more than one standard deviation. This can be explained by the strong correlation between the c quark mass and the Fermi momentum [11]. Greater values of the c quark mass are connected with smaller values of the Fermi momentum.

The value of the Cabibbo-Kobayashi-Maskawa matrix element $|V_{cb}|$ has only marginally increased with the greater branching ratios compared to the free-quark model. This is again due to the smooth square root dependence of $|V_{cb}|$ on the semileptonic branching ratio.

The χ^2 per degree of freedom is in all fits with the ACCMM model closer to 1 than in the free-quark model fits. The two additional free parameters of the ACCMM model enable a better fit to the measured spectra.

ACCMM	e	μ	$\frac{e+\mu}{2}$
$BR\,[\%]$	$9.7 \pm 0.2 \pm 0.6$	$9.8 \pm 0.3 \pm 0.6$	$9.7 \pm 0.2 \pm 0.6$
$\|V_{cb}\| \cdot 10^2$	$4.1 \pm 0.1 \pm 0.3$	$4.2 \pm 0.1 \pm 0.3$	$4.1 \pm 0.1 \pm 0.2$
$m_b\,[GeV/c^2]$	5.02 ± 0.08	4.90 ± 0.09	4.97 ± 0.06
$m_c\,[GeV/c^2]$	1.71 ± 0.07	1.57 ± 0.08	1.65 ± 0.05
$p_F\,[GeV/c]$	0.23 ± 0.07	0.34 ± 0.08	0.27 ± 0.05
χ^2/DoF	53.7/48	37.2/31	92.1/82

Table 3.9: *Results of the fits to the lepton spectra with the ACCMM model. The values of the b quark masses are obtained from Equation 1.9.*

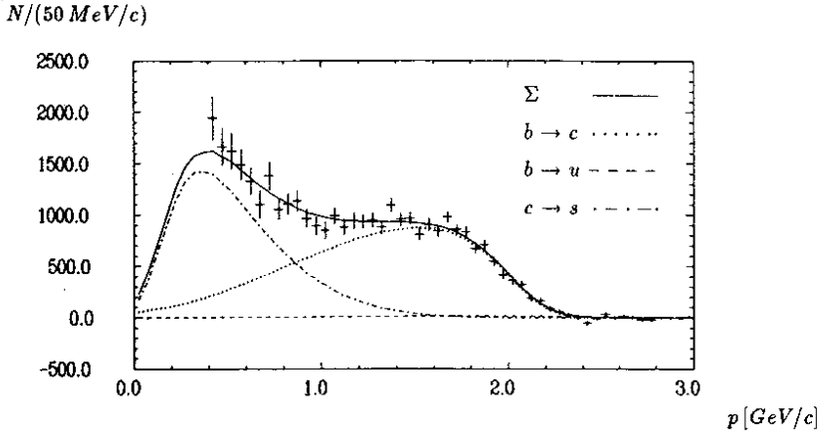

Figure 3.12: *Fit to the corrected $e^{\pm}$ spectrum with the ACCMM model.*

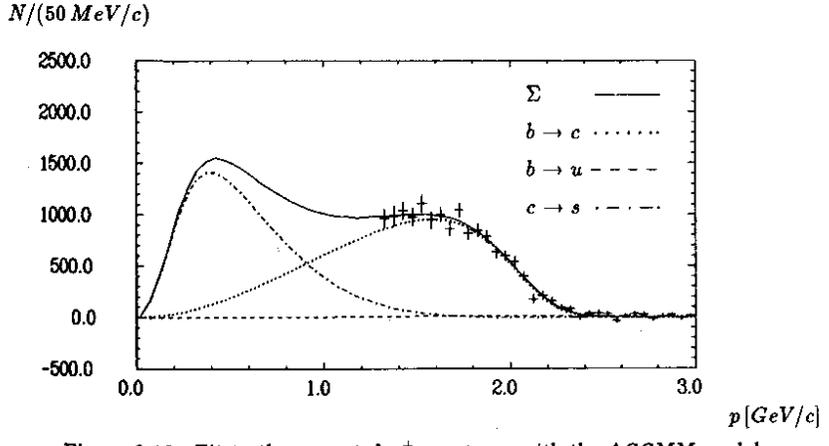

Figure 3.13: *Fit to the corrected $\mu^{\pm}$ spectrum with the ACCMM model.*

3.4.3 GISW Model

The third theoretical model fit to the lepton spectra is the GISW model. The results of the fits are summarized in Table 3.10 and shown in Figures 3.14 and 3.15.

The fits with the GISW model result in a slightly smaller inclusive semileptonic branching ratio than with the ACCMM model. It turns out to be $(9.4 \pm 0.6)\,\%$ in the muon fit and $(9.5 \pm 0.6)\,\%$ in the electron and combined fit. The statistical error results from the same number of fit parameters as in the free-quark model fits.

Although the branching ratio measured with the GISW model is smaller than the one with the ACCMM model, the Cabibbo-Kobayashi-Maskawa matrix element $|V_{cb}|$ has a larger value. The value obtained in all three fits of this Section is $0.042 \pm 0.001 \pm 0.006$. It is compatible within errors with the free-quark and ACCMM models.

The χ^2 per the degree of freedom for each GISW fit is close to 1, as in the ACCMM model.

GISW	e	μ	$\frac{e+\mu}{2}$
$BR\,[\%]$	$9.5 \pm 0.2 \pm 0.6$	$9.4 \pm 0.2 \pm 0.6$	$9.5 \pm 0.1 \pm 0.6$
$\lvert V_{cb}\rvert \cdot 10^2$	$4.2 \pm 0.1 \pm 0.6$	$4.2 \pm 0.1 \pm 0.6$	$4.2 \pm 0.1 \pm 0.6$
χ^2/DoF	53.4/50	37.7/33	91.1/84

Table 3.10: *Results of the fits to the lepton spectra with the GISW model.*

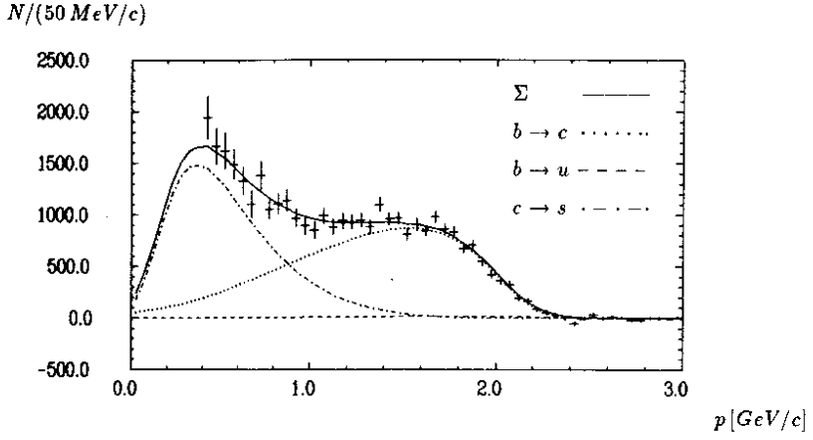

Figure 3.14: *Fit to the corrected $e^{\pm}$ spectrum with the GISW model.*

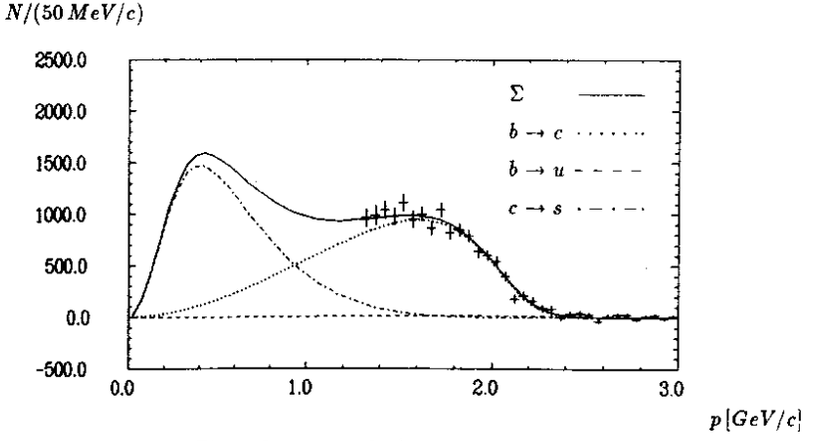

Figure 3.15: *Fit to the corrected $\mu^{\pm}$ spectrum with the GISW model.*

3.4.4 Modified 'GISW' Model: Free Amount of D^{**}

In the original GISW model the proportion of D, D^* and D^{**} mesons in the final state is 27 %, 60 %, and 13 %, respectively. In this Section the ratio of D/D^* mesons is fixed to the value of the GISW model of 0.27/0.60. The amount of D^{**} mesons on the one hand and the sum of the D and D^* mesons on the other are free fit parameters. The fit function is written as:

$$\left(\frac{dN}{dp}\right)^{exp} = a\left[0.27\left(\frac{dN}{dp}\right)^{B\to Dl\nu} + 0.60\left(\frac{dN}{dp}\right)^{B\to D^*l\nu}\right] + b\left(\frac{dN}{dp}\right)^{B\to D^{**}l\nu} + c\left(\frac{dN}{dp}\right)^{c\to s} + d\left(\frac{dN}{dp}\right)^{b\to u} \quad (3.22)$$

This modification of the GISW model is made in order to find out if the semileptonic branching ratio and, therefore, $|V_{cb}|$ change with an added degree of freedom in the 'GISW' model. It is not meant as a means of measuring $B \to D^{**}l\nu$. The background from $B \to D^*\pi l\nu$ is hard to determine and should look in the lepton spectra like $B \to D^{**}l\nu$ decays. The results of the fits are summarized in Table 3.11 and shown in Figures 3.16 and 3.17.

'GISW' (free D^{**})	e	μ	$\frac{e+\mu}{2}$
$B \to D, D^*l\nu$ [%]	$7.9 \pm 0.3 \pm 0.5$	$7.7 \pm 0.4 \pm 0.5$	$7.9 \pm 0.3 \pm 0.5$
$B \to D^{**}\, l\nu$ [%]	$1.6 \pm 0.5 \pm 0.1$	$1.7 \pm 0.7 \pm 0.1$	$1.6 \pm 0.4 \pm 0.1$
$b \to u$ [%] (fixed)	$0.2 \pm 0.0 \pm 0.0$	$0.2 \pm 0.0 \pm 0.0$	$0.2 \pm 0.0 \pm 0.0$
Σ [%]	$9.7 \pm 0.6 \pm 0.6$	$9.7 \pm 0.8 \pm 0.6$	$9.7 \pm 0.5 \pm 0.6$
$\lvert V_{cb}\rvert \cdot 10^2$	$4.3 \pm 0.2 \pm 0.6$	$4.3 \pm 0.2 \pm 0.6$	$4.3 \pm 0.2 \pm 0.6$
χ^2/DoF	52.9/49	37.1/32	90.1/83

Table 3.11: *Results of the fits to the lepton spectra with a 'GISW' model modified to include a free D^{**} contribution. The $b \to u$ transitions are fixed according to $|V_{ub}|/|V_{cb}| = 0.1$* (see Section 3.4).

The semileptonic branching ratio turns out to 9.7 % in all three fits. The statistical error is increased in comparison to the original GISW model due the greater number of fit spectra. The systematic error of the inclusive semileptonic branching ratio is because of correlations of the single contributions added linearly.

The amount of $B \to D^{**}(D^*\pi)l\nu$ decays comes out to be $(17 \pm 4)\,\%$ of all semileptonic $b \to c$ quark decays in the combined fit to electrons and muons. This is compatible within errors with the value of 13 % quoted in the original GISW model. In this respect, the original GISW model is confirmed.

The value of the Cabibbo-Kobayashi-Maskawa matrix element $|V_{cb}|$ increases only slightly in comparison to the original GISW model value to $0.043 \pm 0.002 \pm 0.006$.

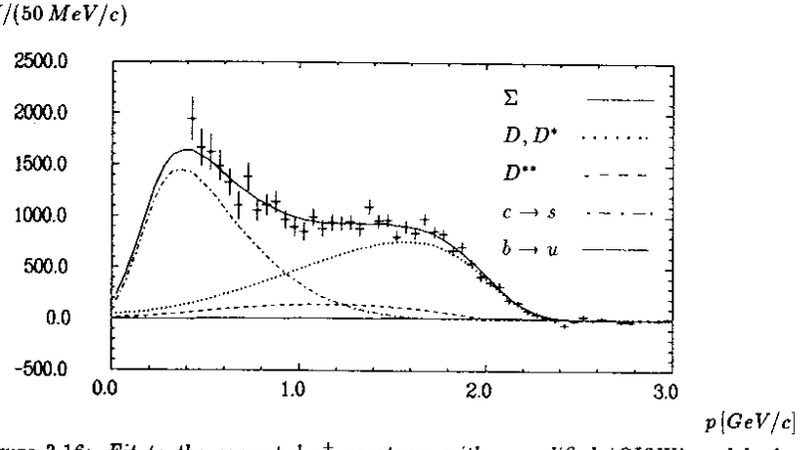

Figure 3.16: *Fit to the corrected $e^{\pm}$ spectrum with a modified 'GISW' model: free amount of D^{**}.*

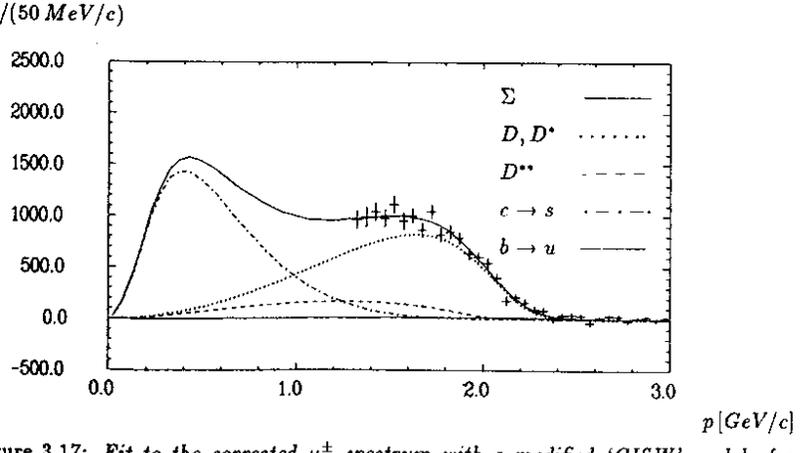

Figure 3.17: *Fit to the corrected $\mu^{\pm}$ spectrum with a modified 'GISW' model: free amount of D^{**}.*

3.4.5 Interpretation of the Results

At this point, the results obtained using the different theoretical models should be interpreted.

The semileptonic branching ratio values vary from 9.4 % with the free-quark model to 9.7 % with the ACCMM and modified 'GISW' models. The original GISW model yields 9.5 %. The statistical errors of the free-quark and the GISW models are small, 0.1 %. For the ACCMM model, those increase to 0.2 % due to the two free parameters of the $b \to c$ lepton spectrum: p_F and m_c. The modified 'GISW' model with free D^{**} amount has the largest statistical error of 0.5 % because of the additional fit curve from the D^{**} contribution. The experimental systematic error of 0.6 % is larger than the statistical one in all models. It is dominated by the uncertainty in the number of B mesons and to a lesser extent by the lepton identification efficiency. The errors arising from the model dependence of the branching ratio have not been quoted so far. The maximum spread in the different model results, 0.3 %, is used as an estimate. This value is larger than the statistical error of most of the models but smaller than the systematic experimental error.

The results on $|V_{cb}|$ range from 0.041 obtained with the free-quark and ACCMM models to 0.043 with the modified 'GISW' model. The value for the GISW model is 0.042. At a level of about 0.001 the experimental errors, comprising the measurement errors and the uncertainty in the B lifetime, are rather small. In contrast to the semileptonic branching ratio, the theoretical uncertainties on $|V_{cb}|$ are in general larger than the experimental errors. In the spectator models, they result from uncertainties in the quark masses and lie at 0.002 in both cases. In the formfactor models, they are due to uncertainties in the chosen wave functions. The errors on $|V_{cb}|$ in these models are 0.006. A more precise value of $|V_{cb}|$ can only be obtained from the inclusive lepton spectrum with a better theoretical description of B meson decays.

Larger values of $|V_{cb}|$ have been reported in a recent ARGUS paper [25]. $|V_{cb}|$ is obtained by fitting the q^2 spectrum of the decay $\bar{B}^0 \to D^{*+}l^-\nu_l$ on the basis of the Heavy Quark Effective Theory [6,24]. Values for $|V_{cb}|$ vary from $0.045 \pm 0.005 \pm 0.003$ to $0.053 \pm 0.008 \pm 0.003$ depending on the Isgur-Wise function chosen to fit the q^2 distribution.

Although the results of the semileptonic branching ratio measurement are in good agreement and the errors due to the theoretical models small, the model dependencies cause further uncertainties. An approach to determine a 'model independent' semileptonic branching ratio value is described in the following Chapter.

Chapter 4

'Model-Independent' Inclusive Semileptonic Branching Ratio of B Mesons with D Tagging

In the work of Chapter 3, theoretical models were necessary to measure the inclusive semileptonic branching ratio of B mesons. These models introduce further uncertainties into the analysis, and the measured branching ratios are model dependent.

In this Chapter, a method is described which determines the semileptonic branching ratio without any need of a theoretical description of the primary lepton spectrum. The advantage of this method is, therefore, 'model independence', although there is a deterioration in statistics.

4.1 Method

The reason why theoretical models had to be used to determine the semileptonic branching ratio in the work of Chapter 3 is the strong contribution from semileptonic D meson decays in the measured lepton spectra. A suppression of these secondary decays would allow one to dispense with theoretical descriptions of the lepton spectra.

The suppression of semileptonic D decays can be done as follows. Leptons coming from B decays can be tagged by measuring D mesons from the other decaying B in the event. The principle is shown in Equation 4.1:

$$\begin{aligned} B^0 &\rightarrow X\, \mathbf{D^{*-}} \\ \bar{B}^0 &\rightarrow Y\, \mathbf{e^-}\bar{\nu}_e,\ Y \rightarrow Z\, e^+\nu_e\,. \end{aligned} \tag{4.1}$$

An e^- coming from a $\bar{B}^0$ decay is tagged by a D^{*-}, whereas a $D^{*-}e^+$ combination shows an e^+ coming from a secondary D meson decay. The statistics can be improved by using not only $D^{*-}e^-$ combinations but also $D^{*-}\mu^-$, $\bar{D}^0 e^-$, and $\bar{D}^0\mu^-$ combinations as well as their charged conjugated systems.

The branching ratios of inclusive D meson production in B decays as well as the D branching ratios are rather uncertain. Therefore, only a relative measurement is done. The ratio of the number of leptons in the momentum interval $[1.2-3.0]\,GeV/c$ to the number of leptons in the entire kinematically allowed momentum interval $[0.0-3.0]\,GeV/c$ is measured. This cancels out not only the D meson production rates in B decays and D branching ratios but also their reconstruction efficiencies. In order to get the inclusive semileptonic branching ratio of B mesons this is combined

with the number of leptons of the inclusive lepton spectrum in the momentum interval $[1.2-3.0]\,GeV/c$, where the amount of leptons from $c \rightarrow s$ transitions and other backgrounds is almost negligible.

4.2 Lepton Selection

In this method the small statistics of the measured events yields a much larger uncertainty than the systematic error. The cut on the lepton polar angle is, therefore, released compared to the previous method.

$$|\cos\theta| < 0.85\,. \tag{4.2}$$

This results in a larger fake lepton contribution but the gain in statistics is significant. Other than this, the leptons are selected exactly as in Chapter 3.

4.3 D^0 and D^{*+} Selection

The lowest uncertainty in the number of Dl events can be achieved with D^0 and D^{*+} tags. The D^0 and D^{*+} mesons are reconstructed in the following decay modes:

$$\begin{aligned} D^{*+} &\rightarrow D^0\pi^+ \quad (BR = (55\pm 4)\,\%\,[31])\,, \\ D^0 &\rightarrow K^-\pi^+ \quad (BR = (3.65\pm 0.21)\,\%\,[31])\,. \end{aligned} \tag{4.3}$$

Their inclusive production rates in B meson decays are:

$$\begin{aligned} B &\rightarrow D^{*+}X \quad (BR = (26.9\pm 3.5)\,\%\,[31])\,, \\ B &\rightarrow D^0X \quad (BR = (46\pm 5)\,\%\,[31])\,. \end{aligned} \tag{4.4}$$

In order to get a good signal to background ratio and a simple signal description the following cuts for the D^0 reconstruction are applied. The K^- and π^+ candidates are selected with the combined likelihood of the dE/dx and ToF measurements:

$$LH_{K,\pi}^{dE/dx,ToF} \geq 0.05\,. \tag{4.5}$$

For a precise momentum and dE/dx measurement in the drift chamber the charged particles have to travel through at least 25 wire layers. The angles of the K^- and π^+ mesons relative to the beam axis have to be:

$$|\cos\theta_{K,\pi}| \leq 0.85\,. \tag{4.6}$$

A further reduction of combinatorical background is achieved with restricting the angle of the K^- momentum θ_K^* in the reference system of the D^0 meson to:

$$\cos\theta_K^* < 0.8\,. \tag{4.7}$$

The D^0 candidates for the D^{*+} reconstruction have to fulfill further conditions. The mass of the $K\pi$ combination has to be close to nominal mass from [31]:

$$\begin{aligned} |m(K\pi) - m(D^0)| &< 80\,MeV/c^2 \text{ and} \\ \chi_D^2 &< 16 \end{aligned} \tag{4.8}$$

where

$$\chi^2_D = \frac{(m(K\pi) - m(D^0))^2}{\sigma^2(m)} \tag{4.9}$$

and $m(K\pi)$ is the mass of the $K\pi$ combination, $\sigma(m)$ the error on $m(K\pi)$, and $m(D^0)$ the mass from [31]. In order to improve the D^0 momentum resolution the four momentum vector is fit with the following constraint:

$$E^2(K\pi) - (\vec{p}(K\pi))^2 = m^2(D^0) \tag{4.10}$$

where E and $\vec{p}$ are the measured energy and momentum of the $K\pi$ combination. The criteria for the slow pion coming from the decay $D^{*+} \to D^0\pi^+$ are loose:

$$\begin{aligned} |\cos\theta_\pi| &< 0.92\,, \\ LH_\pi^{dE/dx,ToF} &> 0.01\,. \end{aligned} \tag{4.11}$$

The continuum contribution to the invariant mass spectra can be suppressed without effecting the signal. The scaled momentum x_p of the D^0 or D^{*+} candidates is restricted to the maximum allowed value in B decays:

$$x_p(D^0, D^{*+}) \leq 0.5\,, \tag{4.12}$$

with

$$x_p \equiv p/p_{max}\,, \quad p_{max} = \sqrt{E^2_{Beam} - m^2_D}\,. \tag{4.13}$$

The invariant mass spectra of the D^0 and the D^{*+} candidates accompanied by e^+ candidates in the momentum range $0.4\,GeV/c \leq p_e \leq 3.0\,GeV/c$ and their charged conjugated systems are shown in Figures 4.1 and 4.2, respectively.

4.4 Fitting Procedure for D^0 and D^{*+} Candidates

D^0 Candidates

Since a K^+ can fake a π^+ and a π^- can fake a K^-, a $\bar{D}^0$ meson can fake a D^0 meson. This leads to signal for $\bar{D}^0$ mesons in the mass distribution of D meson candidates. Therefore, it is necessary to include in the fit function of the D^0 candidates a background of $\bar{D}^0$ candidates and vice versa. The fit function for the $D^0 l^+$ and $\bar{D}^0 l^-$ candidates, respectively, looks like:

$$\begin{aligned} f_{K^-\pi^+(l^+)}(m) &= N(D^0)\cdot s + p\cdot N(\bar{D}^0)\cdot s_{mid} + b_3 \\ \text{and}\quad f_{K^+\pi^-(l^+)}(m) &= N(\bar{D}^0)\cdot s + p\cdot N(D^0)\cdot s_{mid} + b'_3 \end{aligned} \tag{4.14}$$

where N is the number of D candidates, s a Gaussian curve, b a polynomial of third order, and p the misidentification probability of $\bar{D}^0$ for D^0 mesons. Because the Equations in 4.14 are coupled, the fit procedure is an iteration process. The constants used in the fit functions are [34]:

Width of the signal s: $\sigma_{D^0} = 14\,MeV/c^2$,
Width of the misidentified signal s_{mid}: $\sigma_{mid} = 40\,MeV/c^2$,
Shift relative to the signal: $\Delta m = -11\,MeV/c^2$,
Misidentification probability: $p = 0.30$.

Because of a reflection from the decay $D \to K\pi\pi$ in the mass interval $1.5\,GeV/c^2 < m(K^-\pi^+) < 1.7\,GeV/c^2$ the invariant mass distribution of the D^0 candidates is only fit in the mass intervals $[1.3 - 1.5]\,GeV/c^2$ and $[1.7 - 2.5]\,GeV/c^2$.

D^* Candidates

The invariant mass spectra of D^{*+} mesons are easier to fit than the D^0 ones. The fit function consists of a Gaussian curve plus the following background [34]:

$$b_{D^0\pi^-}(m) = N_b \cdot m(m - m_0)^{0.75} \cdot e^{-\alpha(m-m_0)} \tag{4.15}$$

where α and N_b are free fit parameters, and $m_0 = 2004\,MeV/c^2$.

4.5 Backgrounds with D^0 and D^{*+} Tagging

There are several backgrounds in Dl^+ events found in $\Upsilon(4S)$ data which have to be corrected. Most are explained in Chapter 3. But some of these need to be corrected in different ways, and a new background, $B^0\bar{B}^0$ mixing, needs to be taken into account. These background corrections are explained in this Section. The number of signal and background events can be found in Table 4.3 for D^0 and in Table 4.4 for D^{*+} tagging, respectively.

Continuum

The continuum background is directly measured in off resonance data below the $\Upsilon(4S)$ resonance. The continuum data are treated exactly like $\Upsilon(4S)$ data. After scaling them according to the luminosities, they are subtracted from the $\Upsilon(4S)$ data.

Fakes

The next source of background are hadrons misidentified as leptons. Fake rates are determined according to Section 3.3.2 with $\Upsilon(1S)$ data. They are averaged over the studied momentum intervals. The rates used in this and the next Chapter are:

Fake Probability [%] in Momentum Interval	e	μ
$[1.2 - 3.0]\,GeV/c$	0.3 ± 0.1	1.5 ± 0.5
$[0.4 - 3.0]\,GeV/c$	0.5 ± 0.1	–

Table 4.1: *Fake probabilities.*

Hadrons, denoted by h^+, are selected as in Section 3.3.2. Dh^+ combinations are treated like Dl^+ combinations. In order to determine the number of faked Dl^+ combinations the Dh^+ combinations are multiplied by the fake rates after continuum subtraction.

$B^0\bar{B}^0$ Mixing

An as yet not mentioned background lies in $B^0\bar{B}^0$ mixing. It introduces a secondary lepton contribution in the tagged sample. Since the mixing parameter, all contributing branching ratios, and all efficiencies (see Section 4.6) are known, the background

can be calculated. If a $\bar{D}$ is reconstructed in the final state the number of background events due to $B\bar{B}$ mixing is:

$$\begin{aligned} N_{Mixing}(Dl^+) &= N_B f_0 \chi BR(B^0 \to \bar{D}) BR(\bar{D} \to f) \eta_D \\ &\times [BR(B^0 \to \bar{D}^0 X) BR(\bar{D}^0 \to X l^-) \\ &+ BR(B^0 \to D^- X) BR(D^- \to X l^-)] \eta_{p_l}^{Sec} \eta_l \end{aligned} \tag{4.16}$$

where f_0 is the fraction of $\Upsilon(4S)$ decays to neutral B mesons and $\chi = (0.16 \pm 0.04)$ the mixing parameter [31]. $\eta_{p_l}^{Sec}$, η_l, and η_D are the efficiencies for the cuts on the lepton momentum, lepton selection, and $\bar{D}$ reconstruction. The semileptonic D meson branching ratios used are:

$$\begin{aligned} D^0 &\to X l^+ \quad (BR = (7.9 \pm 1.1)\,\% \,[31])\,, \\ D^+ &\to X l^+ \quad (BR = (17.2 \pm 1.9)\,\% \,[31])\,. \end{aligned} \tag{4.17}$$

τ Leptons

τ leptons which are produced in B decays and decay to electrons or muons also contribute to the background. This component is subtracted in a manner similar to the $B^0\bar{B}^0$ mixing correction:

$$\begin{aligned} N_\tau(Dl^+) &= N_B BR(B \to \bar{D}) BR(\bar{D} \to f) \eta_D \\ &\times BR(\bar{B} \to \tau^- X) BR(\tau^- \to l^- \bar{\nu}_l \nu_\tau) \eta_{p_l}^{\tau} \eta_l\,. \end{aligned} \tag{4.18}$$

The branching ratio $BR(\bar{B} \to \tau^- X)$ is assumed to be 30 % of the branching ratio $BR(\bar{B} \to e^- X)$ [26].

D_s Mesons

In weak decays of B mesons the virtual W boson can materialize as a D_s meson. D_s mesons can decay semileptonically like D^+ mesons. Because the branching ratio is expected to be small, the decay mode $D_s^+ \to l^+\nu$ is not taken into account. Hence, the resulting background due to semileptonic D_s decays is:

$$\begin{aligned} N_{D_s}(Dl^+) &= N_B BR(B \to \bar{D}) BR(\bar{D} \to f) \eta_D \\ &\times BR(\bar{B} \to D_s X) BR(D_s \to X l \nu) \eta_{p_l}^{D_s} \eta_l\,. \end{aligned} \tag{4.19}$$

The semileptonic branching ratio of D_s mesons is assumed to be $BR(D_s \to X l\nu) = (8.5 \pm 1.3)\,\%$, as calculated from the semileptonic branching ratio and the lifetime of D^+ mesons [31].

J/ψ Mesons

J/ψ mesons which decay to leptons contribute negligibly. For completeness, the number of Dl^+ events due to decaying J/ψ from B mesons is:

$$\begin{aligned} N_{J/\psi}(Dl^+) &= N_B BR(B \to \bar{D}) BR(\bar{D} \to f) \eta_D \\ &\times BR(\bar{B} \to J/\psi X) 2 BR(J/\psi \to l^+ l^-) \eta_{p_l}^{J/\psi} \eta_l\,. \end{aligned} \tag{4.20}$$

4.6 Efficiency and Bremsstrahlung Corrections

Further corrections have to be applied to the Dl^+ sample. They consist of efficiency corrections, momentum extrapolation, and bremsstrahlung corrections.

Efficiencies

The reconstruction efficiencies for D^0 and D^{*+} mesons are determined with Monte Carlo. With the cuts of Section 4.3 they are [34]:

$$\begin{aligned} \eta_{D^0} &= (50.0 \pm 2.5)\,\%, \\ \eta_{D^{*+}} &= (26.5 \pm 2.4)\,\%. \end{aligned} \tag{4.21}$$

The efficiency η_l for lepton selection is a product of the efficiencies for the angular cut, likelihood function acceptance, and track reconstruction probability.

Efficiencies of the lepton momentum cuts η_{p_l} are determined with Monte Carlo. The relative error is assumed to be 5 %. In the case of electrons, bremsstrahlung losses are taken into account before calculating the acceptance of each momentum cut η_{p_l}. The efficiencies are:

Efficiency [%]	e $[0.4-3.0]$ GeV/c	e $[1.2-3.0]$ GeV/c	μ $[1.2-3.0]$ GeV/c
η_l	66.9 ± 1.3	68.5 ± 1.3	61.1 ± 1.2
$\eta_{p_l}^{Prim}$	95.7 ± 4.8	59.9 ± 3.0	68.0 ± 3.4
$\eta_{p_l}^{Sec}$	62.0 ± 3.1	3.4 ± 0.2	4.2 ± 0.2
$\eta_{p_l}^{\tau}$	77.6 ± 3.9	9.0 ± 0.5	11.4 ± 0.6
$\eta_{p_l}^{\Lambda_c}$	61.7 ± 3.1	0.8 ± 0.0	1.0 ± 0.1
$\eta_{p_l}^{D_s}$	56.7 ± 2.8	3.5 ± 0.2	4.3 ± 0.2
$\eta_{p_l}^{J/\psi}$	97.9 ± 4.9	77.9 ± 3.9	87.6 ± 4.4

Table 4.2: *Efficiencies for the lepton selection and momentum cuts.*

Momentum Extrapolation to Zero

The likelihood identification function for electrons recognizes only electrons with momenta above $0.4\,GeV/c$. Hence, the very low momentum part of the spectrum has to be determined through extrapolation. The average of the ACCMM and GISW models is used for this. 4 % of the $b \to c$ lepton spectrum integral is below $0.4\,GeV/c$.

Bremsstrahlung for Muons

In order to improve the statistics muons are also used in the momentum region above $1.2\,GeV/c$. After they are efficiency corrected they are folded with bremsstrahlung effects. The muons can then be treated as 'electrons'.

4.7 Number of Observed Events

The numbers of observed leptons after the cuts of Section 4.3 can be found in Table 4.3 for D^0 and in Table 4.4 for D^{*+} tagging together with the calculated backgrounds and corrections. The systematic errors of the $\Upsilon(4S)$ and continuum data are determined by varying the signal width within the errors found in [22].

$D^0 l^+ / \bar{D}^0 l^-$	e $[0.4-3.0]$ GeV/c	e $[1.2-3.0]$ GeV/c	μ $[1.2-3.0]$ GeV/c
$\Upsilon(4S)$	$331 \pm 37 \pm 8$	$152 \pm 21 \pm 5$	$167 \pm 24 \pm 5$
Scaled Continuum	$8 \pm 35 \pm 8$	$0 \pm 18 \pm 4$	$5 \pm 21 \pm 5$
Fakes	$36 \pm 1 \pm 7$	$2 \pm 0 \pm 1$	$9 \pm 1 \pm 3$
D_s	$11 \pm 0 \pm 4$	$1 \pm 0 \pm 0$	$1 \pm 0 \pm 0$
τ	$8 \pm 0 \pm 6$	$1 \pm 0 \pm 1$	$1 \pm 0 \pm 1$
Mixing	$8 \pm 0 \pm 3$	$0 \pm 0 \pm 0$	$1 \pm 0 \pm 0$
J/ψ	$3 \pm 0 \pm 1$	$2 \pm 0 \pm 0$	$3 \pm 0 \pm 1$
Σ	$257 \pm 53 \pm 16$	$146 \pm 28 \pm 7$	$148 \pm 32 \pm 8$
Efficiency Corrected Σ	$384 \pm 80 \pm 26$	$212 \pm 40 \pm 12$	$215 \pm 47 \pm 15$
Extrapolation to $0.0\,GeV/c$	$399 \pm 83 \pm 27$	–	–
Bremsstrahlung Folded	–	–	$191 \pm 41 \pm 13$

Table 4.3: *Signal and backgrounds for $D^0 l^+$ events.*

$D^{*+} l^+ / D^{*-} l^-$	e $[0.4-3.0]$ GeV/c	e $[1.2-3.0]$ GeV/c	μ $[1.2-3.0]$ GeV/c
$\Upsilon(4S)$	$38.7 \pm 6.8 \pm 2.1$	$17.7 \pm 4.6 \pm 1.3$	$18.4 \pm 4.8 \pm 1.6$
Scaled Continuum	$2.6 \pm 2.6 \pm 0.8$	$0.0 \pm 2.6 \pm 0.8$	$0.0 \pm 2.6 \pm 0.8$
Fakes	$3.1 \pm 0.2 \pm 1.2$	$0.2 \pm 0.1 \pm 0.1$	$0.7 \pm 0.2 \pm 0.3$
D_s	$1.9 \pm 0.0 \pm 0.7$	$0.1 \pm 0.0 \pm 0.0$	$0.2 \pm 0.0 \pm 0.1$
τ	$1.4 \pm 0.0 \pm 1.0$	$0.2 \pm 0.0 \pm 0.1$	$0.2 \pm 0.0 \pm 0.2$
Mixing	$1.3 \pm 0.0 \pm 0.5$	$0.1 \pm 0.0 \pm 0.0$	$0.1 \pm 0.0 \pm 0.0$
J/ψ	$0.5 \pm 0.0 \pm 0.1$	$0.4 \pm 0.0 \pm 0.1$	$0.4 \pm 0.0 \pm 0.1$
Σ	$27.8 \pm 7.3 \pm 2.8$	$16.7 \pm 5.3 \pm 1.6$	$17.2 \pm 5.7 \pm 1.8$
Efficiency Corrected Σ	$41.6 \pm 11.0 \pm 4.4$	$24.5 \pm 8.2 \pm 2.4$	$25.1 \pm 8.0 \pm 2.9$
Extrapolation to $0.0\,GeV/c$	$43.3 \pm 11.4 \pm 4.6$	–	–
Bremsstrahlung Folded	–	–	$22.3 \pm 7.3 \pm 2.6$

Table 4.4: *Signal and backgrounds for $D^{*+} l^+$ events.*

Averaging the number of electrons and 'muons' in the momentum interval $[1.2-3.0]\,GeV/c$ leads to following ratio of the number of electrons in the high momentum region to the total number of electrons:

$$D^0 \text{ Tagging: } \frac{\#\text{ electrons } [1.2-3.0]\,GeV/c}{\#\text{ electrons } [0.0-3.0]\,GeV/c} = 0.51 \pm 0.15 \pm 0.04\,, \qquad (4.22)$$

$$D^{*+} \text{ Tagging: } \frac{\#\text{ electrons } [1.2-3.0]\,GeV/c}{\#\text{ electrons } [0.0-3.0]\,GeV/c} = 0.55 \pm 0.27 \pm 0.07\,. \qquad (4.23)$$

4.8 Number of Leptons in the Inclusive Spectrum above $1.2\,GeV/c$

The number of electrons of the inclusive spectrum above a momentum of $1.2\,GeV/c$ can be found in Table 4.5. Although the number of muons is not used in this part of the analysis they are listed here as well. They are needed for charm counting in semileptonic B decays as outlined in the next Chapter.

The numbers of $\Upsilon(4S)$, continuum, and fake leptons are determined by integrating the measured spectra from $1.2\,GeV/c$ to $3.0\,GeV/c$. The backgrounds coming from τ leptons, Λ_c baryons, J/ψ, D, and D_s mesons are calculated according to Equations 4.18 to 4.20, 5.11, and 5.12, respectively, without requiring the reconstruction of D mesons in the final state.

	e	μ
$\Upsilon(4S)$	$24889 \pm 174 \pm 0$	$26805 \pm 180 \pm 0$
Continuum (scaled)	$8803 \pm 166 \pm 102$	$10886 \pm 185 \pm 127$
Fakes	$272 \pm 18 \pm 91$	$625 \pm 28 \pm 208$
D	$648 \pm 0 \pm 94$	$803 \pm 0 \pm 119$
J/ψ	$271 \pm 0 \pm 44$	$306 \pm 0 \pm 50$
τ	$116 \pm 0 \pm 78$	$148 \pm 0 \pm 99$
D_s	$86 \pm 0 \pm 26$	$106 \pm 0 \pm 32$
Λ_c	$7 \pm 0 \pm 3$	$9 \pm 0 \pm 4$
$B \to X l \nu$	$14682 \pm 242 \pm 197$	$13922 \pm 260 \pm 304$
Efficiency Corrected	$21424 \pm 353 \pm 702$	$20237 \pm 378 \pm 1027$

Table 4.5: *Number of leptons in the inclusive spectrum above $1.2\,GeV/c$.*

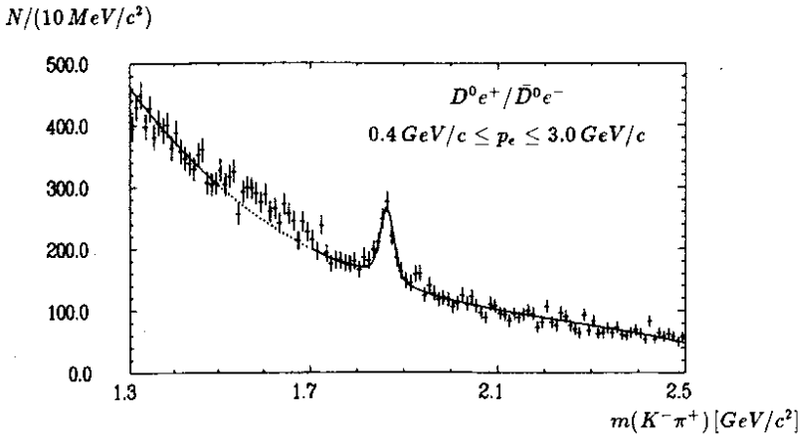

Figure 4.1: *Invariant mass spectrum of D^0 candidates accompanied by e^+ candidates, $0.4\,GeV/c \leq p_e \leq 3.0\,GeV/c$.*

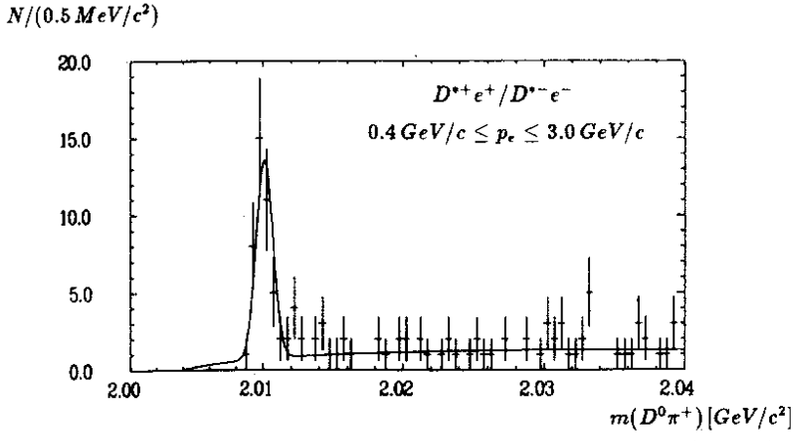

Figure 4.2: *Invariant mass spectrum of D^{*+} candidates accompanied by e^+ candidates, $0.4\,GeV/c \leq p_e \leq 3.0\,GeV/c$.*

4.9 The 'Model-Independent' Semileptonic Branching Ratio of B Mesons

Averaging the ratios of electrons and 'muons' in the momentum interval $[1.2 - 3.0]\,GeV/c$ to all electrons obtained with D^0 and D^{*+} tagging leads to following number:

$$\frac{\#\text{ electrons }[1.2-3.0]\,GeV/c}{\#\text{ electrons }[0.0-3.0]\,GeV/c} = 0.53 \pm 0.15 \pm 0.04\,. \tag{4.24}$$

This is compatible within errors with the value of the GISW model. After boosting the electrons from the B meson reference frame into the laboratory frame and adding corrections for bremsstrahlung and momentum resolution the GISW model gives:

$$\frac{\#\text{ electrons }[1.2-3.0]\,GeV/c}{\#\text{ electrons }[0.0-3.0]\,GeV/c} = 0.62\,. \tag{4.25}$$

Combining the ratio of electrons above $1.2\,GeV/c$ to all electrons with the number of electrons of the inclusive spectrum above $1.2\,GeV/c$ leads to a 'model independent' inclusive semileptonic branching ratio of B mesons of:

$$BR(B \to Xe\nu) = (11.2 \pm 2.8 \pm 1.1)\,\%\,. \tag{4.26}$$

This 'model independent' inclusive semileptonic branching ratio mesons is larger than the branching ratios obtained by fitting theoretical models to lepton spectra, but well in agreement within errors.

A 'model independent' value of $|V_{cb}|$ can not be obtained from the 'model independent' semileptonic branching ratio. Quark masses have to be used to calculate $|V_{cb}|$ from Equation 1.6. The masses used are $m_b = 5.0\,GeV/c^2$ and $m_c = 1.7\,GeV/c^2$, i.e. the masses used in the free-quark model of Chapter 3. The absolute value of the quark mass dependent Cabibbo-Kobayashi-Maskawa matrix element V_{cb} turns out to be:

$$|V_{cb}| = 0.045 \pm 0.006 \pm 0.002\,. \tag{4.27}$$

This value is compatible within errors with the value of $|V_{cb}|$ obtained by fitting theoretical models to the inclusive lepton spectrum. The experimental error, the first quoted error, is now dominated by the statistical uncertainty in the inclusive semileptonic branching ratio. The theoretical error is due the uncertainties in the quark masses equal to the error on $|V_{cb}|$ of the free-quark model.

Chapter 5

D Meson Fraction in Semileptonic B Meson Decays

There are two reasons to measure the D meson fraction of the final state of semileptonic B decays. First, it is of interest to know whether there is a baryonic contribution to the hadrons in the final state. Second, the charm fraction in semileptonic B decays is an indirect measurement of charmless B decays.

The theoretical models which are used to fit the lepton spectra in the analysis of Chapter 3 describe only of D mesons in the final hadronic state. These models can, therefore, only be applied if it can be proven that there are only mesons in the final state and no baryons.

The expected charm fraction of semileptonic B decays can easily be calculated in the spectator model. If one takes $|V_{ub}|/|V_{cb}| = 0.1$, the phase space factors, and gluon corrections from Equation 3.20, one ends up with a charm fraction of 98 %. Therefore, one expects in the absence of baryons that in 98 % of all semileptonic B decays a D^0 or a D^+ meson will emerge in the final state.

5.1 Method

Charm counting in the final state of semileptonic B decays is done with D^0 and D^+ mesons. Excited D mesons like D^* or D^{**} do not decay by weak interaction and so they do not produce any lepton. They decay by strong or electromagnetic interactions and produce a D^0 or D^+ meson in the final state.

In order to count the charm fraction in semileptonic B decays one has to be sure that the lepton and the D meson come from the same B. Possible lepton D meson combinations are indicated in Equation 5.1:

$$\begin{aligned} B^0 &\rightarrow X\, \mathbf{D}^- l^+ \nu \\ \bar{B}^0 &\rightarrow Y\, D^+ \pi^- \,,\; D^+ \rightarrow Z l^+ \nu \,. \end{aligned} \tag{5.1}$$

Only a $D^- l^+$ or a $D^0 l^-$ combination where the lepton is fast guarantees that the D meson and the lepton come from the same B.

5.2 Lepton Selection

Leptons are selected with the same likelihood and angular cuts as in the measurement of the 'model-independent' inclusive semileptonic branching ratio of B mesons outlined in Chapter 4. A momentum cut for electrons and muons of $p_l > 1.2\,GeV/c$ is chosen. This suppresses leptons from semileptonic decays of the unreconstructed D meson. Furthermore it allows the comparison of the charm fraction of the electron and muon data samples directly.

5.3 D^0 and D^+ Selection

D^0 mesons are selected exactly as indicated in Chapter 4. D^+ mesons are selected similarly to D^0 mesons. They are reconstructed in the following decay mode:

$$D^+ \rightarrow K^- \pi^+ \pi^+ \quad (BR = (8.0^{+0.8}_{-0.7})\,\%\,[31]). \tag{5.2}$$

The inclusive production rate of D^+ mesons in B meson decays is:

$$B \rightarrow D^+ X \quad (BR = (22.7 \pm 3.3)\,\%\,[31]). \tag{5.3}$$

The K^- and π^+ candidates are selected with the combined likelihood of the dE/dx and ToF measurements:

$$LH_{K,\pi}^{dE/dx,ToF} \geq 0.05\,. \tag{5.4}$$

In order to keep the reconstruction efficiency of D^+ mesons high the the polar angle of the kaons and pions is opened up compared to the cut for reconstructing D^0 mesons:

$$|\cos\theta_{K,\pi}| < 0.90 \;\text{ for }\; D^+ \rightarrow K^- \pi^+ \pi^+\,. \tag{5.5}$$

Again a further reduction of combinatorical background is reached through restricting the angle of the K^- momentum θ_K^* in the reference system of the D^+ meson to

$$\cos\theta_K^* < 0.8\,, \tag{5.6}$$

The scaled momentum x_p of the D^+ candidates coming from B decays is restricted to be less than the maximum kinematically allowed value:

$$x_p(D^+) \leq 0.5\,, \tag{5.7}$$

The reconstruction efficiency for D^+ candidates turns out to be:

$$\eta_{D^+} = (40 \pm 2)\,\%\,. \tag{5.8}$$

The invariant mass spectrum of the D^0 and the D^+ candidates accompanied by e^- candidates in the momentum range $1.2\,GeV/c \leq p_e \leq 3.0\,GeV/c$ and their charged conjugated systems are shown in Figures 5.1 and 5.2, respectively.

5.4 Fitting Procedure for D^0 and D^+ candidates

The fitting procedure for D^0 mesons has already been described in Chapter 4. The mass spectra of the D^+ candidates is fit with the following function:

$$f_{K^-\pi^+\pi^+(l^-)}(m) = N(D^+)\cdot s(D^+) + N(D^{*+})\cdot s(D^{*+}) + b_2 \tag{5.9}$$

where N is the number of mesons, s the signal width, and b_2 a polynomial second degree. The signal width for the D^+ candidates is $12\,MeV/c^2$, as determined by Monte Carlo [34]. The width of the reflection from D^{*+}, which can be clearly seen in Figure 5.2 at $2.01\,GeV/c^2$, is free. Because of a reflection from the decay $D \rightarrow K\pi\pi\pi$, the fit is only made between $1.7\,GeV/c^2$ and $2.5\,GeV/c^2$.

5.5 Backgrounds with D^0 and D^+ Tagging

The backgrounds in D meson counting are similar to the backgrounds in the measurement of the 'model-independent' inclusive semileptonic branching ratio of B mesons. Continuum, fakes, τ leptons, D_s, and J/ψ mesons are treated exactly as in Chapter 4. $B^0\bar{B}^0$ mixing, semileptonic D and Λ_c meson decays are treated as follows:

$B^0\bar{B}^0$ Mixing

$B^0\bar{B}^0$ mixing can produce a D^0l^- or a D^+l^- combination where the D and the lepton come from different B mesons. The number of these events is calculated with:

$$\begin{aligned} N_{Mixing}(Dl^+) &= N_B f_0 \chi BR(B^0 \rightarrow \bar{D}) BR(\bar{D} \rightarrow f) \eta_D \\ &\times BR(B^0 \rightarrow Xl^+\nu) \eta_{p_l}^{Prim} \eta_l \,. \end{aligned} \tag{5.10}$$

Semileptonic D Meson Decays

Since the unreconstructed D meson can decay semileptonically, D^0l^- or D^+l^- combinations can occur where the lepton comes from a D instead of the correct B meson. The number of these background events is:

$$\begin{aligned} N_{Sec}(Dl^+) &= N_B BR(\bar{B} \rightarrow D) BR(D \rightarrow f) \eta_D \\ &\times [BR(B \rightarrow \bar{D}^0 X) BR(\bar{D}^0 \rightarrow Xl^-) \\ &+ BR(B \rightarrow D^- X) BR(D^- \rightarrow Xl^-)] \eta_{p_l}^{Sec} \eta_l \,. \end{aligned} \tag{5.11}$$

Semileptonic Λ_c Baryon Decays

Semileptonic Λ_c decays can be treated analogously to semileptonic D meson decays. The number of Dl^+ events due to Λ_c decays is:

$$\begin{aligned} N_{\Lambda_c}(Dl^+) &= N_B BR(\bar{B} \rightarrow D) BR(D \rightarrow f) \eta_D \\ &\times BR(B \rightarrow \Lambda^- X) BR(\Lambda^- \rightarrow Xl^-\bar{\nu}) \eta_{p_l}^{\Lambda_c} \eta_l \,. \end{aligned} \tag{5.12}$$

5.6 Number of Observed Events

The number of observed $\Upsilon(4S)$ D^0l^- and D^+l^- events where the lepton momentum is above $1.2\,GeV/c$, together with the backgrounds can be found in Tables 5.1 and 5.2, respectively. In order to calculate the D meson fraction, these numbers have to be corrected for the branching ratio of the D meson to the measured final state, the D meson reconstruction efficiency, and the inclusive production rate of D mesons in B decays. Dividing the number of corrected D^0l^- or D^+l^- events by the number of $B \rightarrow Xl\nu$ leptons in the inclusive spectrum (Table 4.5) gives the D meson fraction of semileptonic B decays in the final state.

	D^0e^-	$D^0\mu^-$
$\Upsilon(4S)$	$204.0 \pm 23.1 \pm 5.1$	$245.5 \pm 25.3 \pm 6.1$
Continuum (scaled)	$15.5 \pm 16.8 \pm 3.6$	$0.0 \pm 19.4 \pm 4.4$
Fakes	$3.7 \pm 0.5 \pm 1.2$	$14.9 \pm 1.9 \pm 3.7$
Mixing	$9.8 \pm 0.0 \pm 2.9$	$11.1 \pm 0.0 \pm 3.4$
D	$5.4 \pm 0.0 \pm 1.2$	$6.7 \pm 0.0 \pm 1.5$
J/ψ	$2.3 \pm 0.0 \pm 0.5$	$2.6 \pm 0.0 \pm 0.6$
τ	$1.0 \pm 0.0 \pm 0.7$	$1.2 \pm 0.0 \pm 0.9$
D_s	$0.7 \pm 0.0 \pm 0.2$	$0.9 \pm 0.0 \pm 0.3$
Λ_c	$0.1 \pm 0.0 \pm 0.0$	$0.1 \pm 0.0 \pm 0.0$
Σ	$165.6 \pm 28.4 \pm 7.5$	$208.0 \pm 32.1 \pm 10.1$
Efficiency Corrected Σ	$241.6 \pm 41.5 \pm 13.3$	$302.3 \pm 46.7 \pm 20.4$

Table 5.1: *Number of D^0e^- and $D^0\mu^-$ events for charm counting.*

	D^+e^-	$D^+\mu^-$
$\Upsilon(4S)$	$181.2 \pm 32.9 \pm 9.1$	$137.1 \pm 34.5 \pm 9.5$
Continuum (scaled)	$34.3 \pm 23.5 \pm 7.7$	$0.0 \pm 29.2 \pm 9.5$
Fakes	$3.5 \pm 1.1 \pm 1.2$	$13.3 \pm 4.5 \pm 2.7$
Mixing	$8.4 \pm 0.0 \pm 2.8$	$9.6 \pm 0.0 \pm 3.2$
D	$4.7 \pm 0.0 \pm 1.3$	$5.8 \pm 0.0 \pm 1.7$
J/ψ	$2.0 \pm 0.0 \pm 0.5$	$2.2 \pm 0.0 \pm 0.6$
τ	$0.8 \pm 0.0 \pm 0.6$	$1.1 \pm 0.0 \pm 0.8$
D_s	$0.6 \pm 0.0 \pm 0.2$	$0.8 \pm 0.0 \pm 0.3$
Λ_c	$0.0 \pm 0.0 \pm 0.0$	$0.1 \pm 0.0 \pm 0.0$
Σ	$126.8 \pm 40.6 \pm 12.7$	$104.2 \pm 45.2 \pm 15.1$
Efficiency Corrected Σ	$185.0 \pm 59.3 \pm 19.5$	$151.5 \pm 65.7 \pm 23.2$

Table 5.2: *Number of D^+e^- and $D^+\mu^-$ events for charm counting.*

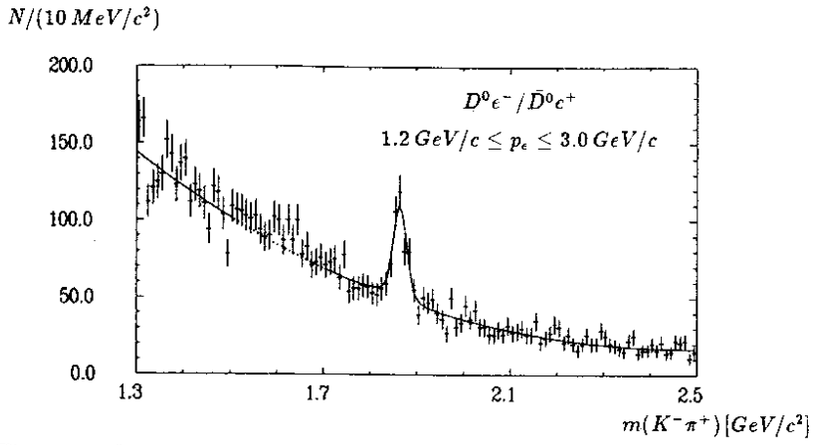

Figure 5.1: *Invariant mass spectrum of D^0 candidates accompanied by e^- candidates, $1.2\,GeV/c \leq p_e \leq 3.0\,GeV/c$.*

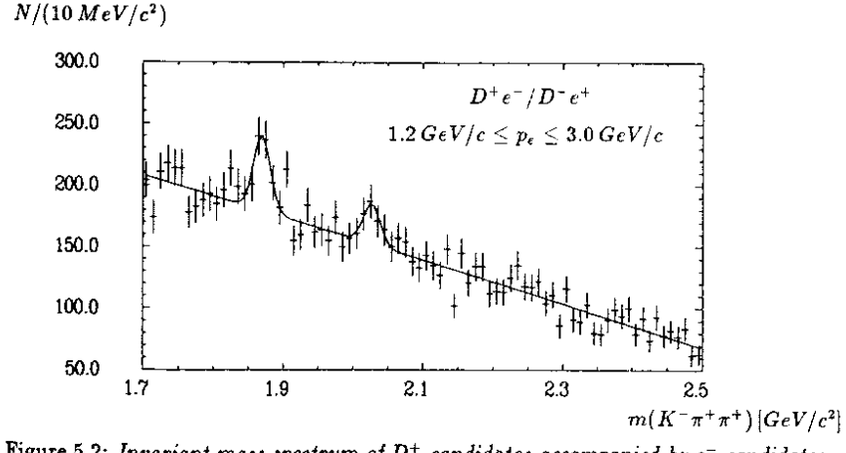

Figure 5.2: *Invariant mass spectrum of D^+ candidates accompanied by e^- candidates, $1.2\,GeV/c \leq p_e \leq 3.0\,GeV/c$. The peak at $2.01\,GeV/c^2$ results from a reflection of D^{*+} decays.*

5.7 The D Meson Fraction of Semileptonic B Decays

The D^0 and D^+ meson fractions of semileptonic B decays, along with their sums, are listed in Table 5.3. Averaging electron and muon events above $1.2\,GeV/c$, the D meson fraction of semileptonic B decays is determined to be $(97 \pm 14)\,\%$.

D Meson Fraction [%]	e	μ	$\frac{e+\mu}{2}$
$\frac{BR(B \to XD^0l^-)}{BR(B \to Xl^-)}$	$62 \pm 11 \pm 6$	$82 \pm 13 \pm 8$	$72 \pm 8 \pm 7$
$\frac{BR(B \to XD^+l^-)}{BR(B \to Xl^-)}$	$27 \pm 9 \pm 4$	$23 \pm 10 \pm 5$	$25 \pm 7 \pm 4$
$\frac{BR(B \to XDl^-)}{BR(B \to Xl^-)}$	$89 \pm 14 \pm 8$	$105 \pm 16 \pm 10$	$97 \pm 11 \pm 8$

Table 5.3: *D meson fraction in semileptonic B decays with lepton momenta greater than $1.2\,GeV/c$.*

Two comments should be made: First, semileptonic B decays are saturated by D meson production. There is no need for a baryon contribution to the final state. Therefore, the theoretical models described in Chapter 1 can be applied to fit the lepton spectra in Chapter 3. Second, the value of $|V_{ub}|$ is confined to be small. A D meson fraction of $(97 \pm 14)\,\%$ in semileptonic B decays is compatible with $|V_{ub}|/|V_{cb}| = 0.1 \pm 0.01$, as measured by [9].

Summary

To conclude, the inclusive semileptonic branching ratio of B mesons have been measured both model dependently and 'model independently'. The D meson fraction in the final state of semileptonic B decays has been determined.

Table 5.4 summarizes the results of the inclusive semileptonic ranching ratio of B mesons and $|V_{cb}|$. The averaged model dependent branching ratio is plotted in Figure 5.3 with a filled symbol and can be compared to older measurements with open symbols.

Model	$BR(B \to Xl\nu)$ [%]	$\lvert V_{cb}\rvert \cdot 10^2$
Free-Quark Model	$9.4 \pm 0.1 \pm 0.6$	$4.1 \pm 0.1 \pm 0.2$
ACCMM	$9.7 \pm 0.2 \pm 0.6$	$4.1 \pm 0.1 \pm 0.2$
GISW	$9.5 \pm 0.1 \pm 0.6$	$4.2 \pm 0.1 \pm 0.6$
'GISW' (free D^{**})	$9.7 \pm 0.5 \pm 0.6$	$4.3 \pm 0.2 \pm 0.6$
'Model Independent'	$11.2 \pm 2.8 \pm 1.1$	$4.5 \pm 0.6 \pm 0.2$

Table 5.4: *Inclusive semileptonic branching ratio of B mesons and $|V_{cb}|$.*

The inclusive semileptonic branching ratio of B mesons as determined with different theoretical models are in good agreement. The smallest branching ratio is measured with the free-quark model, $(9.4 \pm 0.1 \pm 0.6)\,\%$. The largest are obtained with the ACCMM model, $(9.7 \pm 0.2 \pm 0.6)\,\%$ and the modified 'GISW' model with free D^{**} amount, $(9.6 \pm 0.5 \pm 0.6)\,\%$. The original GISW model yields $(9.5 \pm 0.1 \pm 0.6)\,\%$.

The uncertainty in the model dependent inclusive semileptonic branching ratios is dominated by the systematic errors, due mainly to the number of B mesons. The differences in the semileptonic branching ratios as determined by the different theoretical models are less than the experimental systematic uncertainties.

The absolute values for the Cabibbo-Kobayashi-Maskawa matrix element V_{cb}, as determined using the various theoretical models, are in good agreement. The smallest one is obtaind with the free-quark and ACCMM models, $0.041 \pm 0.001 \pm 0.002$, the largest with the modified version of the GISW model with free D^{**} amount, $0.043 \pm 0.002 \pm 0.006$. The value from the original GISW model, $0.042 \pm 0.001 \pm 0.006$, lies between those of the free-quark and ACCMM models on the one hand and the modified version of the GISW model on the other.

The error on the Cabibbo-Kobayashi-Maskawa matrix element $|V_{cb}|$, obtained by fitting theoretical models to the lepton spectrum, is dominated by theoretical uncertainties, the second quoted error on $|V_{cb}|$. In the ACCMM and free-quark models, these are caused by uncertainties in the quark masses. In the GISW model, they are due to uncertainties in the chosen wave functions [20]. The experimental error, the first quoted error, consists of the of the B lifetime and the errors of this measurement.

The 'model independent' semileptonic branching ratio of $(11.2 \pm 2.8 \pm 1.1)\,\%$ and the quark mass dependent value of $|V_{cb}|$ of $0.045 \pm 0.006 \pm 0.002$ calculated from that are larger than values obtained from the model fits to the lepton spectra but compatible within errors. The errors in both values are dominated by the statistical uncertainty.

Taking into account all experimental and model uncertainties, the measured inclusive semileptonic branching ratio is substantially lower than the value of $(12 - 16)\,\%$ predicted by pure spectator models [33]. But they are well within the range estimated by a more recent work including non-spectator diagrams of B decays. The most plausible candidate is W exchange with gluon emission which suppresses semileptonic decays of neutral B mesons.

The D meson content of the final state of semileptonic B decays for lepton momenta greater than $1.2\,GeV/c$ is summarized in Table 5.5. The D meson fraction of $(97 \pm 14)\,\%$ suggests that there are only mesons produced in semileptonic B decays. Furthermore it confirms that the charmless B decay fraction is small.

D Meson Fraction [%]	$\frac{e+\mu}{2}$
$\frac{BR(B \to XD^0 l^-)}{BR(B \to Xl^-)}$	$72 \pm 8 \pm 7$
$\frac{BR(B \to XD^+ l^-)}{BR(B \to Xl^-)}$	$25 \pm 7 \pm 4$
$\frac{BR(B \to XDl^-)}{BR(B \to Xl^-)}$	$97 \pm 11 \pm 8$

Table 5.5: *Charm fraction in semileptonic B decays with lepton momenta greater than $1.2\,GeV/c$.*

Comparison with other Measurements

Figure 5.3 compares the inclusive semileptonic branching ratios from different experiments [13,14,15,16,17,18,21,37,39] running on the $\Upsilon(4S)$ resonance. The value from this measurement is plotted with a filled symbol. It is well compatible with more recent results from CLEO [15,16] and ARGUS [21]. The reasons for the differences in the semileptonic branching ratio between older and recent measurements can not be found.

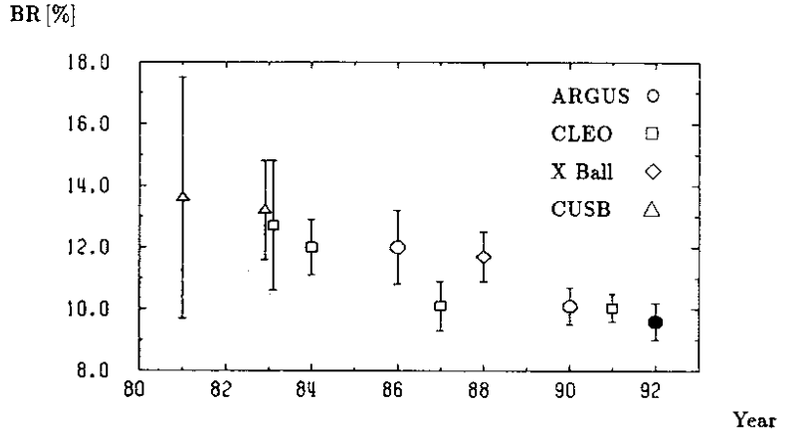

Figure 5.3: *Inclusive semileptonic branching ratio of B mesons measured by different collaborations running on the $\Upsilon(4S)$ resonance* [13,14,15,16,17,18,21,37,39].

Bibliography

[1] G. Altarelli, N. Cabibbo, G. Corbo, L. Maiani, G. Martinelli, Nucl. Phys. **B208**, 365 (1982)

[2] G. Altarelli, S. Petrarca, Phys. Lett. **B261**, 303 (1991)

[3] H. Albrecht et al. (ARGUS), Nucl. Instr. and Meth. **A275**, 1 (1989)

[4] H. Albrecht et al. (ARGUS), DESY 92 - 029, (1992)

[5] H. Albrecht et al. (ARGUS), Z. Phys. **C55**, 25 (1992)

[6] S. Balk, F. Hussain, J. G. Körner, G. Thompson, MZ-TH-92-22 (1992)

[7] J.C. Gabriel, ARGUS Software Note 50, not published

[8] M. Wirbel, B. Stech, M. Bauer, Z. Phys. **C29**, 637 (1985)

[9] H. Albrecht et al. (ARGUS), Phys. Lett. **B234**, 409 (1990)

[10] N. Cabibbo and L. Maiani, Phys. Lett. **79B**, 109 (1978)

[11] J. C. Carlos (ARGUS), Dissertation, Universität Heidelberg, IHEP-HD/89-1 (1988)

[12] B. Gittelman and S. Stone (CLEO), CLNS 87/81 (1987)

[13] K. Chadwick et al. (CLEO), Phys. Rev. **D27**, 475 (1983)

[14] A. Chen et al. (CLEO), Phys. Rev. Lett. **52**, 1084 (1984)

[15] S. Behrends et al. (CLEO), Phys. Rev. Lett. **59**, 407 (1987)

[16] S. Henderson et al. (CLEO), Cornell preprint CLNS 91/1101 (1991)

[17] L. J. Spencer et al. (CUSB), Phys. Rev. Lett. **47**, 771 (1981)

[18] C. Klopfenstein et al. (CUSB), Phys. Lett. **130B**, 444 (1983)

[19] B. Fomynikh (ARGUS), private communication

[20] N. Isgur, D. Scora, B. Grinstein, B. Wise, Phys. Rev. **D39**, 799 (1989)

[21] H. Albrecht et al. (ARGUS) Phys. Lett. **B249**, 359 (1990)

[22] G. Harder (ARGUS), Dissertation, Universität Hamburg, Interner Bericht DESY F15-89-01 (1989)

[23] H. Albrecht et al. (ARGUS), Z. Phys. **C52**, 353 (1991)

[24] N. Isgur, Phys. Rev. **D43**, 810 (1991)

[25] H. Albrecht et al. (ARGUS), DESY 92 - 146 (1992)

[26] R. Kowalewsky, Semi-Leptonic B Meson Decay, Dissertation, Cornell University, 1989

[27] J.G. Körner, G.A. Schuler, Z. Phys. **C46**, 93 (1990)

[28] J. P. Leveille, Proceedings of a CLEO Collaboration Workshop, Cornell preprint CLNS 51/505 (1981)

[29] R. Waldi, ARGUS Software Note 28, not published

[30] A. Nippe (ARGUS), Dissertation, Universität Hamburg, Interner Bericht DESY F15-90-05 (1990)

[31] Particle Data Group, Review of Particle Properties, Physical Review **D45**, Part 2, June 1992

[32] F. Schöberl, H. Pietschmann, Europhysics Letters **2**, 583 (1986)

[33] R. Rückl, Habilitationsschrift, München, 1983

[34] F. Sefkow (ARGUS), Dissertation, Universität Hamburg, Interner Bericht DESY F15-90-04 (1990)

[35] M. A. Shifman, Int. J. Mod. Ph. **A**, Vol. 3 No. 12, 2769 (1988)

[36] H. Gennow (ARGUS), DESY Internal Report F15-85-02, 1985

[37] K. Wachs (Crystal Ball), Dissertation, Universität Hamburg, Interner Bericht DESY F31-88-01 (1988)

[38] F. Wartenberg, Diplomarbeit, Universität Hamburg, Interner Bericht DESY F15-90-02 (1990)

[39] S. Weseler (ARGUS), Dissertation, Universität Heidelberg, IHEP-HD/86-02 (1986)

Acknowledgments

I want to thank all members of the ARGUS collaboration, especially those who were nice to me.

In particular, I thank my colleagues Thorsten "Mole" Kirchhoff for showing me the night life in Hamburg, Thomas Hamacher for entertaining us, Roland Hofmann for being normal, and Patrick Saull four improving my bad english.

H. Schröder I want to thank for the critical discussions of my work, his tips, and ideas.

And last but not least, I thank W. Schmidt-Parzefall and V. Sörgel for making it possible to do my PhD in the ARGUS collaboration.